



A novel non-aqueous tertiary amine system for low energy CO₂ capture developed via molecular dynamics simulation

Guanchu Lu^a, Zhe Wang^b, Zongyang Yue^a, Luxi Yang^a, Xiaolei Zhang^c, Yi Huang^a, Jianhua Qian^{d,*}, Xianfeng Fan^{a,**}

^a Institute for Materials and Processes, School of Engineering, The University of Edinburgh, Edinburgh EH9 3FB, Scotland, UK

^b School of Energy and Environment & Department of Materials Science and Engineering, City University of Hong Kong, Kowloon Tong, Hong Kong

^c Chemical and Process Engineering, University of Strathclyde, Glasgow G1 1XQ, Scotland, UK

^d School of Petrochemical Engineering, Liaoning Petrochemical University, Fushun, China

ARTICLE INFO

Editor: Z. Bao

Keywords:

Non-aqueous CO₂ absorbents
Low energy regeneration

ABSTRACT

The current technology for capturing CO₂ using alkanolamine aqueous solutions is known for its high energy and capital costs. As a result, developing new absorbents for low-energy CO₂ removal remains a challenge. An additional activator can promote CO₂ absorption performance. However, it is based on experimental screening. In this study, based on molecular dynamic simulation, we have successfully developed a novel and energy-efficient CO₂ absorbent by combining N, N-Dimethylethanolamine (DMEA), and ethylene glycol (EG), with different activators, including ethanolamine (MEA), ethylenediamine (EDA), and piperazine (PZ). The addition of these activators significantly enhances the CO₂ absorption performance of DMEA-based absorbents. Among them, DMEA-PZ-EG exhibits the maximum CO₂ absorption rate and capacity, achieving 6.35 (g-CO₂/(kg-soln.-min.)) and 96.5 (g-CO₂/kg-soln.), respectively, representing a 230.1 % and 206.35 % improvement over 2M DMEA-EG absorbent. Moreover, compared to a 30 wt% MEA solution, the energy consumption of DMEA-based absorbents is reduced by 33.93–51.56 %. The reaction products were characterized using various spectroscopic techniques, including Attenuated Total Reflectance Fourier Transform Infrared spectroscopy (ATR-FTIR), and 1D and 2D Nuclear Magnetic Resonance spectroscopy (¹H and ¹³C NMR). The NMR results confirmed that DMEA becomes protonated after CO₂ absorption in the DMEA-EG mixture. The deprotonation of EG promotes its reaction with CO₂, resulting in the forming of EG carbonates. This assumption has been confirmed by the IR spectrum. Furthermore, the effect of activators on CO₂ absorption has been analysed at the molecular level through molecular dynamics simulation and a new method is proposed to predict the CO₂ absorption performance of non-aqueous solvents. Using non-aqueous DMEA absorbents presents a promising approach for improving CO₂ capture efficiency, reducing energy consumption, and facilitating regeneration.

1. Introduction

Greenhouse gas (GHG) emissions have severe negative impacts on the environment and the sustainable development of the economy. Among these GHGs, CO₂ is the most abundant, accounting for nearly 80 % of global GHG impact. From 1975 to 2018, the atmospheric CO₂ concentration increased from 331 to 410 parts per million (ppm) [1,2]. The 2021 Glasgow Agreement (COP 26) aimed to keep the global

average temperature above pre-industrial levels to less than 2 °C by the end of the century while encouraging efforts to limit the increase to 1.5 °C [3]. Achieving this target requires advancing more effective technologies for capturing carbon dioxide (CO₂) with a low energy penalty. At present, post-combustion flue gas treatment by aqueous alkanolamine absorbents is a mature and widely used technology for CO₂ absorption [4]. Among these amines, 30 wt% aqueous MEA solution is generally considered a benchmark solvent because of its low cost and

Abbreviations: DMEA, Dimethylethanolamine; MEA, Monoethanolamine; EG, Ethylene glycol; PZ, Piperazine; EDA, Ethylenediamine; NMF, N-methylformamide; NMR, Nuclear magnetic resonance; vdW, van der Waals; ATR, Attenuated total reflection; HMQC, Heteronuclear Multiple Quantum Coherence; DEGMEE, 2-(2-Ethoxyethoxy)ethanol; DSC, Differential Scanning Calorimetry; TGA, Thermogravimetric Analyzer; FT-IR, Fourier-transform infrared spectroscopy.

* Corresponding author.

** Corresponding author.

E-mail addresses: qianjianhualn@163.com (J. Qian), X.Fan@ed.ac.uk (X. Fan).

<https://doi.org/10.1016/j.seppur.2024.128996>

Received 20 May 2024; Received in revised form 22 July 2024; Accepted 26 July 2024

Available online 27 July 2024

1383-5866/© 2024 The Authors. Published by Elsevier B.V. This is an open access article under the CC BY license (<http://creativecommons.org/licenses/by/4.0/>).

high reactivity with CO₂. However, the regeneration of the solutions is the most significant impediment to broad CCS application due to its high energy penalty, in the range of 3.7–4.2 Kj/g CO₂. The corrosion and thermal degradation of CO₂-loaded Monoethanolamine (MEA) are also problems [5].

Among the various amine absorbents, aqueous primary or secondary amines form fairly stable carbamate with a fast CO₂ absorption rate but quite low CO₂ absorption loading (Theoretically 0.5 mol CO₂ per mole amine). In contrast, tertiary amines form an unstable carbamate, and an alternative reaction forms a bicarbonate ion. Consequently, tertiary amines have a higher theoretical capacity of 1 mol of CO₂ per mole of amine [6,7]. Furthermore, large energy consumption limits the application of these aqueous amine absorbents. Recently, developing new absorbents by replacing water with organic solvents and modifying intermolecular interactions have attracted the attention of academics and industry. Non-aqueous CO₂ absorbents have been shown to be an effective technique for reducing the energy cost of the regeneration process. Organic solvents, including alcohols [8–10], glycols [11–15], glycol ethers [16–19], glymes [20], pyrrolidones [21,22], formamides [23,24], and sulfoxides [25–27] have proven to be a promising solution for reducing regeneration energy. These are due to their lower specific heat capacity, lower heat of vaporization, and higher boiling points compared to water [28]. Glycols like ethylene glycol (EG), diethylene glycol (DEG), and triethylene glycol (TEG) have been a topic of great interest in organic solvents due to their superior thermal stability and low saturated vapour. In previous research, EG has been mixed with different amines to prepare non-aqueous absorbents, including 2-piperidineethanol (2-PE), 2- amino-2-methyl-1-propanol (AMP), and triethylamine (TEA) [29]. These anhydrous solutions increase the absorption rate and greatly reduce the regeneration energy. The energy consumption of 30 wt% MEA-EG was found to be 36.8 % lower than the conventional aqueous 30 wt% MEA [30,31]. This special desorption performance of glycol-based absorbents may be attributed to the weak bonds formed between hydroxyl groups and CO₂, thus facilitating the decomposition of CO₂-rich absorbents [32].

In this study, we proposed a novel non-aqueous tertiary amine system with superior low energy consumption. DMEA is selected because of its high thermal stability and similar structure to MEA, but it replaces the hydrogen atom with methyl groups ($-\text{CH}_3$) attached to the nitrogen atom [6]. The EG was selected as solvent to formulate the DMEA-EG CO₂ absorbents. We aim to explore the CO₂ capture performance and reaction mechanism of DMEA-based absorbents. In first part experiments, we found that although the DMEA-EG binary absorbents demonstrated excellent regeneration capability under mild conditions, their absorption kinetics and capacity were relatively low. The activator addition strategy (AAS) is taken to enhance the CO₂ capture performance of DMEA-EG binary absorbents [21]. However, screening for effective activators requires intensive experimental work, and an effective method is available to reduce the experimental workload. Therefore, we proposed an activator screening strategy via molecular dynamics (MD) simulation. In our recent research, we noticed that with the CO₂ capture process ongoing, the van der Waals (vdW) solubility parameters decreased to a minimum value and then stabilised. After simulation analysis in conjunction with the experiments, we surprisingly found that this minimum vdW solubility parameter corresponds to the experimental maximum CO₂ loading. With this finding, we tested three different common activators, including piperazine (PZ), ethanolamine (MEA), and ethylenediamine (EDA), in a fixed concentration and particularly tested the activator PZ in different concentrations. Surprisingly, the MD simulation results agreed with the experimental work; as CO₂ absorption progressed, the solubility parameters diminished until reaching a nadir and then increased. The interval between the nadir and the subsequent increase corresponds to the maximum CO₂ loading, as observed experimentally. It is worth noting that our MD simulations focused on static conditions at different stages of the reaction, where CO₂ was introduced into the simulation box in the form of carbamates/

carbonates, bypassing direct chemical reactions between CO₂ molecules and amines (DMEA or other activators). Instead, the simulations only encompassed the diffusion processes between amine-CO₂ products and organic solvent molecules. For example, different reaction stage refers to the proportion of CO₂ bound to amine, which we denote as CO₂ loading. When the CO₂ loading is 0.1, it means that 1/10 of the amine is reacted to CO₂ to form carbamate. Then, based on density functional theory (DFT) calculation, the reason for AAS effectively enhancing the CO₂ absorption capacity of the absorbents can be explained based on solvation free energy changes. The solvation free energies ranked as DMEA-PZ-CO₂ < DMEA-MEA-CO₂ < DMEA-EDA-CO₂ < DMEA-EG-CO₂, the solvation free energies of DMEA⁺/EGCOO⁻ (-76.24 Kj/mol) is much higher than DMEA⁺/Activator/COO⁻ (-131.67 to -142.59 Kj/mol) in EG solvent, which means the DMEA⁺/Activator-COO⁻ have higher solubility (lower solvation free energy) in EG compared to DMEA⁺/EGCOO⁻. Based on the guidance of theoretical calculation, the molar ratios of DMEA and activators are further optimized to achieve the best absorption and desorption performance. Then, the CO₂ absorption rate and capacity, desorption rate and efficiency, cyclic stability, and energy consumption of the absorbents are thoroughly investigated.

Finally, various characterization methods, such as Attenuated Total Reflectance Fourier Transform Infrared spectroscopy (ATR-FTIR), Thermogravimetric Analysis (TGA), and Nuclear Magnetic Resonance spectroscopy (¹H NMR and ¹³C NMR), were employed to investigate the absorption mechanism of DMEA-based absorbents. Additionally, the 2D NMR spectrum of DMEA-PZ-EG was also performed to verify the generated alkyl carbonate and protonated DMEA. The characterisation results showed that the unstable alkyl carbonate formed by EG and CO₂ could reduce the regeneration energy consumption of DMEA-based absorbents. According to these findings, the DMEA-based absorbents demonstrate excellent regeneration efficiency under relatively mild conditions (343–353 K), resulting in a 52 % decrease in energy consumption compared to conventional MEA.

2. Materials and experimental section

2.1. Chemicals

DMEA (purity ≥ 99 %, Fisher Chemical), MEA (purity ≥ 99 %, Sigma-Aldrich UK), EDA (98 %, Acros Organics), EG (99 %, Sigma-Aldrich UK), PZ (99 %, Fisher Chemical). Gases used for absorption and desorption experiments (CO₂ and N₂) were of commercial grade with a minimum purity of 99.99 % (Linde Group UK).

2.2. Experimental procedures

The absorption process uses a quartz reactor and DMEA-based absorbents to capture CO₂; a schematic of the absorption apparatus is shown in Fig. S1. Desorption involves regenerating the CO₂-loaded DMEA solution in the same reactor using microwave irradiation, outlined in Fig. S2. The details can be found in Supporting Information Part 1 [30,31,33]. The whole experimental work was divided into three distinct parts. In the first section, DMEA solutions with different molar ratios of EG were tested by a single CO₂ absorption step to identify the best performance molar ratio of DMEA and EG. Then, MD simulation and quantum calculation are carried out to predict activator performance. After identifying the best molar ratio of the DMEA-EG solution, various activators were tested, with a concentration ranging from 0.5 to 2 mol/L. Then, the solution was regenerated under different temperatures ranging from 323 K to 373 K. Based on the absorption capacity and regeneration performances (quantity of stripped CO₂ and energy consumption), the best solutions were submitted to cyclic absorption-regeneration experiments to mimic the industrial CO₂ capture process. The last part focused on thermal stability, energy consumption calculation, and absorption mechanism.

2.3. Materials characterization

The characterization analysis in this research included TG-DSC Analysis, in-situ ATR-FTIR, rheometer, 1D and 2D NMR (^1H and ^{13}C). The specific experimental setup is available in [Supporting Information Part 3 \[34\]](#).

2.4. Computational calculation

In order to further simulate the actual solution environment, simulation boxes were constructed with CO₂-amine products and solvents at different reaction stages in Materials Studio 2020. After constructing the simulation box, we do the Geometry Optimization, which aims to refine the geometry of a structure until the total energy of the structure is minimized. Following optimization, the simulation proceeds under an NVT ensemble (constant number of particles, volume, and temperature) [24,35]. The total process runs for 1000 ps, and a time step of 1 fs is selected. Running the simulation for 1000 ps allows for sufficient time for molecules to interact and mix, ensuring the system reaches equilibrium, and the total energy stabilizes. Then, considering the pressure influence, an NPT ensemble dynamic (constant number of particles, pressure, and temperature) was taken after the NVT ensemble. The total NPT process runs for 200 ps, and the time step is also 1 fs. The DFT calculations were performed using the Gaussian 09 software package [36], utilizing DFT as a powerful tool to elucidate the solvation free energies. The geometries and frequencies of chemicals were optimized at the B3LYP/6-311+G (d, p) level [37]. The single point energy was optimized at B3LYP/6-311++G (2d, 2p) level using the SMD solvation model [38]. The specifics of the MD simulation methodology and the setup for quantum computational methods can be found in [Supporting Information Part 8](#).

3. Results and discussion

3.1. CO₂ absorption/desorption performance of DMEA-EG absorbents

In accordance with the methodology outlined in [Section 2.4](#), a series of CO₂ absorption experiments were conducted under controlled conditions of room temperature (298 K) and pressure (101.3 kPa) by using DMEA-EG absorbents. [Fig. 1](#) shows the CO₂ absorption capacity and kinetics of the six DMEA-EG absorbents with different DMEA concentrations as a function of absorption time. The results, including CO₂ loading, maximum CO₂ absorption kinetics, CO₂ capacity and t₉₅ are presented in [Table 1](#).

[Table 1](#) provides the effect of DMEA concentration on its effectiveness in capturing CO₂. The results indicate that the efficiency of DMEA in capturing CO₂ decreases with the increase in DMEA concentration. This is evident from the decrease in the mole of CO₂ captured per mole of

Table 1

CO₂ absorption loading, t₉₅ and CO₂ absorption capacity and maximum CO₂ absorption rate of DMEA-EG binary absorbents.

Solution name	n _{CO₂} /n _{amine}	CO ₂ absorption (g-CO ₂ /kg-soln.)	Maximum r _{abs} (g-CO ₂ /(kg-soln.·min.))	t ₉₅ *
1M DMEA-EG	0.441	19.41	1.624	2832
2M DMEA-EG	0.358	31.52	1.922	2778
3M DMEA-EG	0.286	37.81	2.151	2712
4M DMEA-EG	0.242	42.57	2.343	2651
5M DMEA-EG	0.205	45.02	2.560	2607
6M DMEA-EG	0.179	47.16	2.703	2503
30 wt% MEA-H ₂ O (5M MEA)	0.540	116.82	7.039	1493

t₉₅*: The time required to achieve 95 % CO₂ absorption capacity.

amine (n_{CO₂}/n_{amine}).

However, there is an interesting observation regarding the maximum CO₂ absorption rate and capacity. Both CO₂ absorption rate and capacity increase as the concentration of DMEA increases. However, the rate of improvement in both absorption rate and capacity diminishes at higher DMEA concentrations. This indicates that under high DMEA concentration conditions, the reactive sites of DMEA are not being utilized efficiently. In comparison to the 30 wt% MEA-H₂O, the maximum CO₂ absorption rate of DMEA-EG is around 2.5 (g-CO₂/(kg-soln.·min.)), only the one third of that of MEA. Moreover, both the absorption capacity and CO₂ loading are much lower than that of MEA, especially the absorption capacity, even the high concentration DMEA-EG (6M DMEA-EG) absorbents, the CO₂ capacity (47.16 (g-CO₂/kg-soln.)) is less than half that of the MEA (116.82 (g-CO₂/kg-soln.)).

Based on the CO₂ loading (n_{CO₂}/n_{amine}) presented in [Table 1](#), the low-concentration DMEA-EG absorbents, specifically the 1M and 2M solutions, demonstrate a relatively high DMEA utilization efficiency. They achieve a mole ratio of 0.442 and 0.358 mol CO₂ per mole DMEA, respectively. Comparing them to the 1M DMEA/EG solution, the 2M DMEA-EG solution exhibits an increase in CO₂ absorption capacity from 19.41 to 31.52 (g-CO₂/kg-soln.), and the maximum absorption rate increases from 1.624 to 1.922 (g-CO₂/(kg-soln.·min.)), representing approximately a 62.3 % and 20.1 % increase, respectively. This indicates that both CO₂ absorption rate and capacity increase with the portion of DMEA, but less DMEA reacts with CO₂ with its concentration increase. There is some potential to maximize the capacity of the mixture.

Therefore, the 2M DMEA-EG absorbent can be considered the optimal concentration for CO₂ capture, striking a balance between DMEA efficiency and CO₂ absorption capacity.

As previously stated, the mixture containing 2M of DMEA and EG showed superior absorbency compared to the other DMEA and EG solutions. This concentration is, therefore, identified as the optimal choice

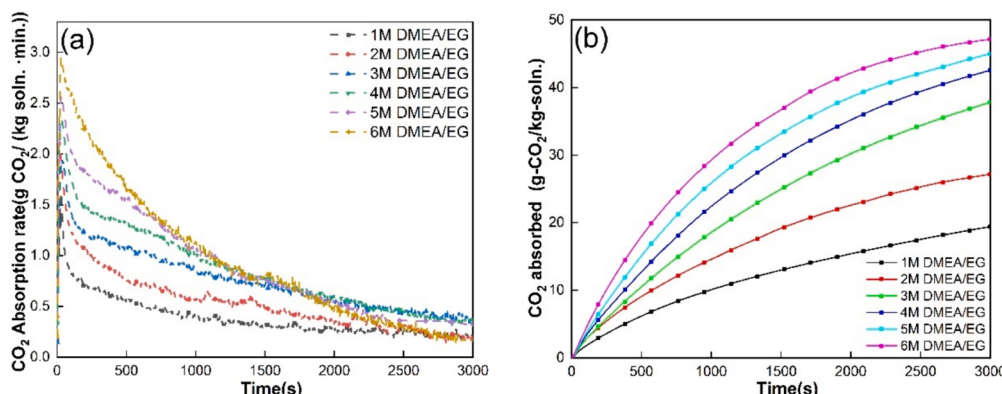


Fig. 1. CO₂ absorption profiles for DMEA-EG mixture with different ratio. (a): CO₂ absorption kinetics (g-CO₂/(kg-soln.·min.)); and (b): CO₂ absorption capacity (g-CO₂/kg-soln.).

for further desorption experiments. To ensure accurate desorption data obtained, CO₂-rich solutions with the 2M DMEA-EG concentration were maintained at a consistent CO₂ loading of 0.36 mol CO₂/mole amine (3.2 wt%) before desorption for all desorption experiments. The desorption time is settled as 3000 s (50 min), as 3000 s is sufficient to ensure full desorption.

Fig. 2 depicts the CO₂ desorption profiles for the 2M DMEA-EG absorbent, showcasing the desorption rate (Fig. 2a) and the amount of CO₂ desorbed (Fig. 2b) when the desorption temperature increased from 323 K to 373 K. While the values of CO₂ desorbed remained relatively constant across the different temperature conditions at the time of 3000 s, the desorption kinetics varied significantly. As presented in Table 2, the maximum desorption rate increased from 1.85 to 24.66 (g-CO₂/(kg-soln·min.)) as the desorption temperature rose from 323 K to 373 K. When the temperature increases from 323 K to 343 K, the maximum desorption rate increases significantly. When the temperature increases from 353 K to 373 K, as shown in Table 2, the maximum desorption rates are in the same range and CO₂ desorption is complete within 500 s. However, the regeneration efficiency only increased from 89.16 % to 94.03 % when the temperature increased from 323 K to 373 K if the desorption time extended to 3000 s.

These findings indicate that the desorption ratio of CO₂-rich DMEA-EG absorbents can reach up to 90 % under mild conditions (333–343 K) [39] when CO₂ is fully desorbed. Increasing the temperature primarily affects the desorption rate, enabling faster desorption, but has little impact on the amount of CO₂ released from DMEA-EG absorbents. Furthermore, the desorption performance of DMEA-EG is different from that of other aqueous amine absorbents. We hypothesised that EG reacts with CO₂ to form the unstable EG alkyl carbonate, where the C—O bond is not as strong as the C—N bond and so can be fully regenerated under mild conditions. The presence of EG alkyl carbonate is confirmed by NMR spectroscopy in Section 3.8. For DMEA-EG absorbents, regenerated at mild conditions (323 K–333 K) takes a longer time and increases energy consumption. To further clarify the relationship between regeneration temperature and energy consumption, we defined the EC₉₅, exhibited the energy/released CO₂ ratio at the time of 95 % CO₂ released, and presented in Table 2. The lowest EC₉₅ is not presented at 323 K, the EC₉₅ value decreases and then increases as the temperature rises, the lowest EC₉₅ value occurred between 333 and 343 K. This result shows that the optimum desorption temperature for DMEA-EG is around 343 K. Although low temperature (323–333 K) desorption can release most of CO₂, it takes a longer time and increases the EC₉₅ values. High temperature (353–373 K) desorption can desorb CO₂ quickly but it consumes too much energy to raise the temperature and results in a high EC₉₅ value as well. In comparison, the 30 % MEA aqueous solution, the desorption efficiency is only 56.9 % under the same desorption setup at 363 K [34]. These indicate that CO₂ is weakly bonded to DMEA-EG absorbents to form carbonate species, which was different from the

carbamate-forming pathway of the aqueous amine absorbents. It aligned with assumptions made in previous studies [39–41].

$$EC = \frac{Energy(kJ)}{CO_2\text{stripped}(mol)} \quad (1)$$

3.2. The activator screening via MD simulation and DFT calculation

In Section 3.1, we examined the CO₂ absorption and desorption behaviour of binary DMEA-EG. The outcomes revealed that the relatively weak bond formed between CO₂ and DMEA-EG facilitates efficient regeneration under mild temperatures (323 K–333 K). However, the limitation of this DMEA-EG system is the low CO₂ absorption capacity and rate. Notably, the CO₂ loading of 2M DMEA-EG was only 0.358 mol CO₂ per mole of amine, significantly lower than the 0.58 loading achieved by 30 wt% MEA [25]. The advantage of the DMEA-EG system is its low regeneration temperature; the weakness is its low absorption capacity. Hence, improving the absorption capacity of DMEA-EG is important. In our study, we noticed that DMEA-EG absorbents saturated with CO₂ still contained a significant amount of unreacted amine and EG, and the reaction products might cease to dissolve in the glycol phase, thereby limiting CO₂ absorption [41]. Some activators may promote further CO₂ absorption in the system. In this section, an Activator Addition Strategy (AAS) [42] is proposed to screen activators to improve the CO₂ absorption performance of DMEA-based absorbents.

Traditionally, activator screening requires extensive experimental efforts [43]. To streamline activator screening, we developed a robust and expedient screening method based on MD simulations. By constructing the simulation box and running the molecular dynamics, we computed the average solubility parameters (vdW solubility) at various absorption stages [44]. It is noteworthy that MD simulations conducted in this study differ from traditional CO₂ absorption MD simulations involving chemical reactions. Our simulations focused on static conditions at different stages of reactions, where CO₂ was introduced into the simulation box in the form of carbamates/carbonates, thus bypassing direct chemical reactions between CO₂ molecules and amines [45]. Instead, the simulations only encompassed the diffusion processes between amine-CO₂ products and organic solvent molecules. Under these circumstances, equilibrium could be achieved in a relatively short simulation time (10 ps) [44].

As CO₂ absorption progressed, vDW solubility decreased until stay relatively stable. For instance, in the case of 2M DMEA-EG, depicted in Fig. 3(a), the vDW solubility decreased from 13.607 (at 0 CO₂ loading) to 12.998 (at 0.3 CO₂ loading) and then slightly increased to 13.157 (at 0.4 CO₂ loading), subsequently, the vDW solubility remained relatively stable around 13.3 until the CO₂ loading reaches to 1.0. This observation implies that the MD simulations predict the CO₂ loading of 2M DMEA-EG ranges from 0.3 to 0.4, aligning well with experimental results (0.358). Consequently, this MD simulation approach holds the potential

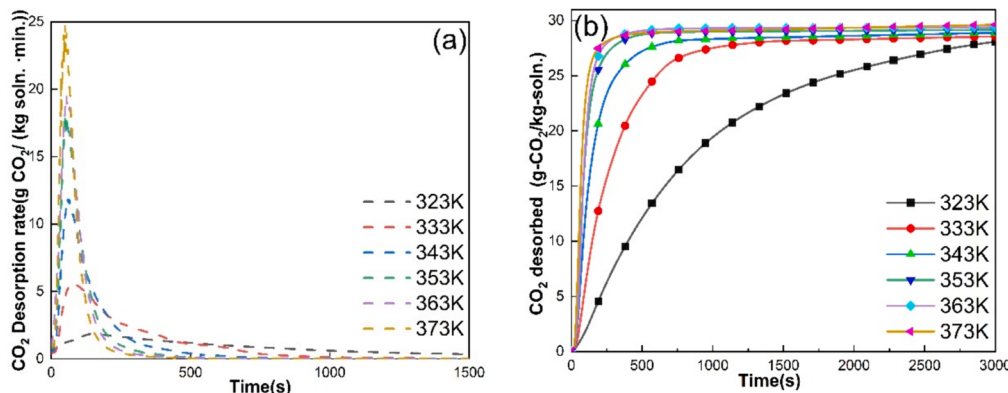


Fig. 2. CO₂ desorption profiles for 2M DMEA-EG; (a): CO₂ desorption rate (g-CO₂/(kg-soln·min.)), and (b): CO₂ desorbed (g-CO₂/kg-soln.).

Table 2

CO_2 desorption loading, t_{95} and maximum desorption rate of 2M DMEA-EG absorbents under different temperature.

Desorption Temperature (K)	CO_2 desorption (g- CO_2 /kg-soln.)	Maximum r_{des} (g- CO_2 /(kg-soln.-min.))	Desorption Ratio (%)	t_{95}^* (s)	Energy Consume (KJ)	EC_{95}^{**} (KJ/mol)
323	27.95	1.85	89.16 %	2380	6.304	2085.16
333	28.56	5.57	90.68 %	881	6.014	1947.44
343	28.89	11.83	91.72 %	533	6.806	2181.96
353	29.17	18.15	92.59 %	305	7.862	2496.56
363	29.38	19.52	93.28 %	249	8.009	2525.16
373	29.62	24.66	94.03 %	221	8.130	2534.84

t_{95}^* : The time required to achieve 95% CO_2 desorption.

EC_{95}^{**} : The Energy per CO_2 in KJ/mole, as defined by Equation (1). The energy and CO_2 desorption value are taken at the time of t_{95} .

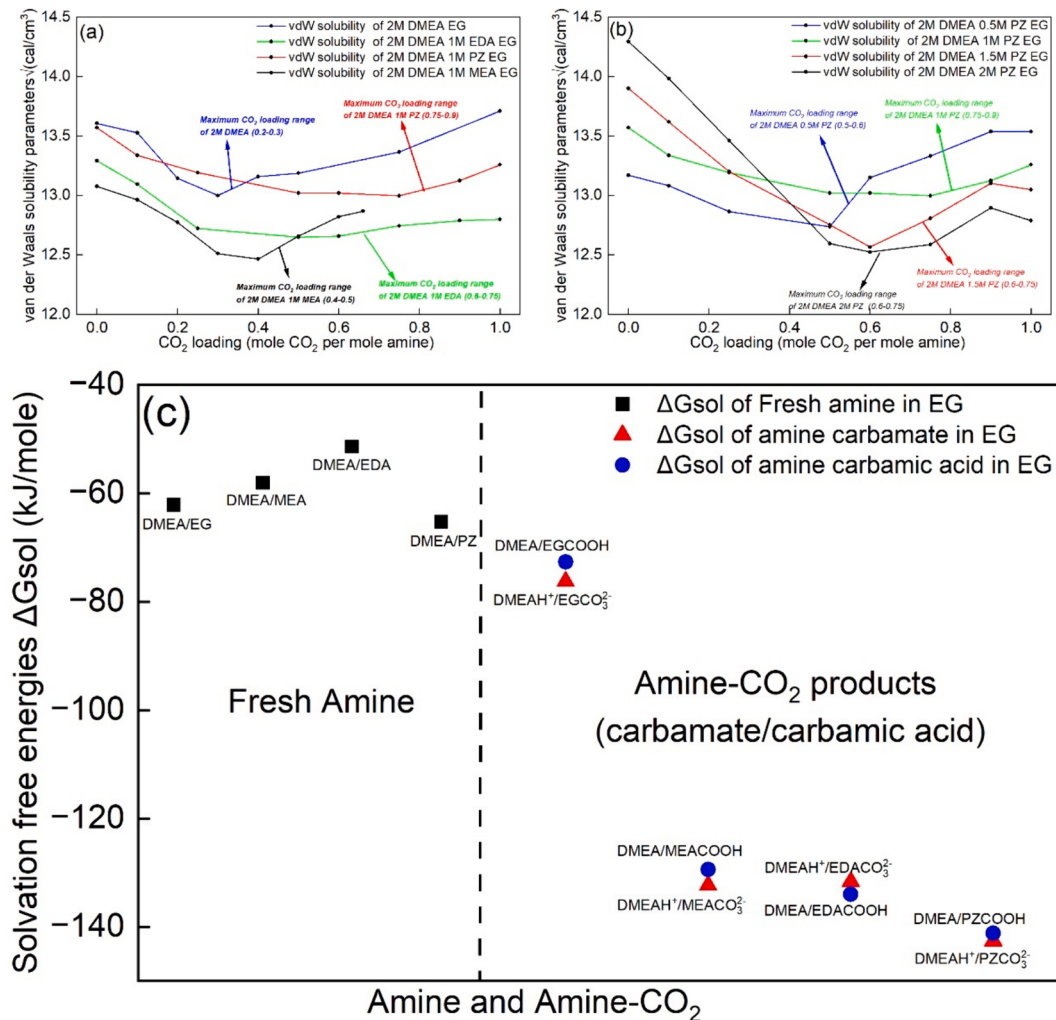


Fig. 3. The results of MD simulation and DFT calculation. (a) vdW solubility of DMEA-EG, DMEA-MEA-EG, DMEA-EDA-EG and DMEA-PZ-EG at different CO_2 loading. (b) vdW solubility of various molar ratio of DMEA to PZ at different CO_2 loading. (c) Solvation free energies of fresh amine (left) and amine- CO_2 products (right) in EG.

for activator screening in DMEA-based absorbents.

Fig. 3(a) also illustrate the vdW solubility parameters trends of 2M DMEA- 1M PZ-EG, 2M DMEA-1M EDA-EG and 2M DMEA-1M MEA-EG. The CO_2 loading of 2M DMEA-EG, 2M DMEA- 1M PZ-EG, and 2M DMEA-1M EDA-EG ranged from 0 to 1.0, but for 2M DMEA-1M MEA- EG, due to the only one primary amine at MEA, the CO_2 loading ranged from 0 to 0.66. The vdW solubility of these absorbents demonstrated similar trends: with the CO_2 loading increased, the vdW solubility decreased until it reached the equilibrium, and the value at which equilibrium is reached is the maximum CO_2 absorption loading measured experimentally. In the MD simulation, the prediction for the maximum CO_2 loading

range of DMEA-PZ-EG was around 0.75, and similar observations and predictions were found for DMEA-EDA-EG (around 0.6) and DMEA-MEA-EG (around 0.4). These predictions range closely matched experimental values: 0.731 CO_2 loading for 2M DMEA- 1M PZ-EG, 0.670 CO_2 loading for 2M DMEA-1M EDA-EG, and 0.435 CO_2 loading for 2M DMEA-1M MEA-EG in experiment measurement. Notably, 2M DMEA-1M PZ-EG displayed the most favourable CO_2 capture performance.

The concentration of added activator also has a significant impact on CO_2 capture performance. In Fig. 3(b), we investigated the CO_2 absorption performance of 2M DMEA-PZ-EG with PZ concentrations ranging from 0.5M to 2M. The vdW solubility also showed consistent

trends, decreasing with rising CO₂ absorption loading until equilibrium. The prediction of CO₂ absorption loading by MD simulation aligns well with the experimental findings. Hence, MD methods offer a means to screen activators efficiently, reducing the experimental workload required for discovering novel non-aqueous CO₂ absorbents. At the same time, this MD simulation method does not need to simulate the whole CO₂ uptake process, but only the diffusion of amine-CO₂ products in the solvent at different CO₂ absorption stages (CO₂ loading), which greatly reduces the time and complexity of MD simulation. However, this MD simulation can only predict the approximate range of CO₂ absorption loading by non-aqueous amines, and the MD simulation is cannot predict the CO₂ desorption performance, which is another criterion for the CO₂ capture performance.

To validate the impact of solubility on non-aqueous CO₂ absorbents, we conducted solvation free energy (ΔG_{sol}) calculations for diverse amine-CO₂ products. The ΔG_{sol} and solubility are two physical properties commonly used to describe the solvation effect. The vdW solubility is getting from the vdW intermolecular potential, which presented the contribution of vdW forces between the solvent and solute molecules. In this MD simulation, COMPASS forcefield is taken to describe the intermolecular potential, which could be expressed as [46–48]:

$$E_{\text{pot}} = \sum_{i>j} \frac{q_i q_j}{r_{ij}} + \sum_{i>j} \epsilon_{ij} \left[2 \left(\frac{r_{ij}^0}{r_{ij}} \right)^9 - 3 \left(\frac{r_{ij}^0}{r_{ij}} \right)^6 \right] \quad (2)$$

A detailed explanation of Eq. (2) is available at [Supporting Information Part 8](#). Solvation free energy is the change in free energy associated with the transfer of a molecule between the ideal gas and a solvent, which conducted from DFT calculation. Without considering the evaporation free energies, the solvation free energies indicate of solubility, which means the lower solvation free energy takes higher solubility. In DMEA-based absorbents, we use the solvation free energy calculated under the same conditions to explain the difference in solubility.

In Fig. 3(c), the left side showed the solvation free energies of fresh amine in EG, and the values are ranged from -51.36 to -65.24 KJ/mol, presenting the similar solubility of unreacted amine in EG. The right side showed the CO₂ loaded amine. For amine-CO₂ products, we considered the amine carbamate and amine carbamic acid as the main components, and solvation free energies consistent solubility hierarchy: DMEA-PZ-CO₂ > DMEA-MEA-CO₂ > DMEA-EDA-CO₂ > DMEA-EG-CO₂. This sequence aligns with both of MD simulations and experimental results, the DMEA-EG absorbents showed the lowest CO₂ loading and DMEA-PZ-EG showed the highest. For DMEA-based absorbents, the theoretical maximum CO₂ loading could reach 1.0 for DMEA-EG, DMEA-PZ-EG and DMEA-EDA-EG, 0.66 for DMEA-MEA-EG. However, the CO₂ loading measured in the experiment is significantly lower than the theoretical maximum value (DMEA-EG 0.36, DMEA-PZ-EG 0.73 DMEA-EDA-EG 0.67 DMEA-MEA-EG 0.435). Discrepancies between theoretical and experimental maximum CO₂ loading in DMEA-based absorbents primarily stem from variations in EG solubility for distinct amine-CO₂ products. These results are explored through a synergy of theoretical and experimental studies. The subsequent experimental design is formulated to validate this activator screening method.

3.3. Ternary DMEA-activator-EG absorbents

3.3.1. Absorption/desorption performance

Following the discussion in [Section 3.1](#), the CO₂ absorption and desorption performance of 2M DMEA-EG were investigated. The results revealed that the weak bond formed between CO₂ and DMEA-EG allows easy regeneration under mild temperatures (323 K–333 K). However, the CO₂ absorption capacity and rate were found to be limited. The CO₂ loading of 2M DMEA-EG is only 0.35 mol CO₂ per mole amine, much lower than 30 wt% MEA (0.58) [25]. To enhance the CO₂ capture performance of DMEA-based absorbents, an AAS strategy was proposed.

In this research, the primary amine MEA, cyclic amine PZ, and diamine EDA were chosen as activators [49,50]. Three different DMEA-Activator-EG blends were formulated with varying molar ratios of the activators, ranging from 0.5M to 2M. [Fig. 4](#) presents the CO₂ absorption capacity and absorption rate of the DMEA-Activator-EG ternary absorbents. Compared to the DMEA-EG binary absorbents, the DMEA-PZ-EG, DMEA-EDA-EG, and DMEA-MEA-EG blends exhibited more than doubled absorption rate, and their CO₂ absorption capacity increased by 1.5–4 times. A similar trend was observed in the CO₂ absorption performance of different DMEA-Activator-EG absorbents. As the CO₂ absorption process progressed, the absorption rate decreased due to the reduction in the number of free amine molecules, which resulted in fewer effective collisions between absorbents and CO₂.

[Table 3](#) provides the absorption data for absorption capacity, maximum absorption rate, t₉₅, and CO₂ rich loading. Among the three DMEA-Activator-EG absorbents, DMEA-PZ-EG demonstrated the best CO₂ capture performance. The CO₂ maximum absorption rate and absorption capacity of DMEA-PZ-EG (2–1) were 6.35 g·CO₂/(kg-soln·min.) and 96.5 (g·CO₂/kg-soln.), respectively, showing a 230.1 % and 206.35 % improvement over 2M DMEA-EG absorbent. As shown in [Table 3](#), as the concentration of activators increased in the DMEA-based absorbents, the CO₂ loading initially increased to a specific value before decreasing. The highest CO₂ loading ($n_{\text{CO}_2}/n_{\text{amine}}$) was observed at a molar ratio of 2:1 for DMEA to activator, reaching 0.731 (DMEA-PZ), 0.670 (DMEA-EDA), and 0.435 (DMEA-MEA), respectively. Similar to the DMEA-EG binary absorbents, a high CO₂ loading ($n_{\text{CO}_2}/n_{\text{amine}}$) indicates a high utilization of amine. Therefore, a concentration of 2M DMEA with 1M activator could be considered the optimal concentration for CO₂ capture, striking a balance between CO₂ loading ($n_{\text{CO}_2}/n_{\text{amine}}$) and CO₂ absorption capacity. In comparison the absorption kinetics with 30 wt% MEA-H₂O, the overall absorption performance of 2M DMEA-2M PZ-EG is better than that of MEA, especially the absorption loading, which is 20.1 % higher.

The results indicate that most of the amino group (—NH—) in activators are reactive and can effectively promote the reaction rate and capacity. Notably, the absorption performance of DMEA blends with PZ or EDA outperformed those of DMEA blends with MEA. This difference can be attributed to the number of —NH— groups in the activators. MEA has only one —NH— group, while PZ and EDA have two. Furthermore, the results for DMEA-PZ blends were superior to those for DMEA/EDA blends, even though both PZ and EDA have the same number of —NH— groups. This distinction may arise from differences in molecular structure. PZ, in particular, rapidly forms bi-carbamate under low CO₂ loading [51].

The desorption performance of DMEA-PZ-EG, DMEA-EDA-EG, and DMEA-MEA-EG with a molar ratio of DMEA: Activator of 2:1 (2–1) was further investigated to assess the CO₂ desorption capabilities of these absorbents. [Fig. 5](#) illustrates the desorption performance of these absorbents at different temperatures ranging from 323 K to 373 K. Additionally, the desorption profiles of DMEA-EG absorbents with varying concentrations of activators are available in [Supporting Information Figs. S5–S10](#).

As shown in [Fig. 5](#), with the desorption temperature increasing from 323 K to 373 K, the maximum desorption rate increased from 6.41 to 37.95 (g·CO₂/(kg-soln. min.)), 3.88 to 30.78 (g·CO₂/(kg-soln. min.)), and 4.96 to 25.62 (g·CO₂/(kg-soln. min.)) for PZ, MEA, and EDA as activators, respectively. Similar as the DMEA-EG binary absorbents, DMEA-Activator-EG blends demonstrated the ability to regenerate under a mild temperature. At a desorption temperature of 343 K, the CO₂ regeneration efficiency reached 70.0 %, 64.9 %, and 81.6 % for DMEA-PZ-EG, DMEA-EDA-EG, and DMEA-MEA-EG, respectively. Furthermore, as the desorption temperature exceeded 343 K, the increase in CO₂ release due to elevated temperature gradually diminished. For instance, compared to 343 K, the regeneration efficiency at 373 K only increased by 15.4 %, 23.5 %, and 4.1 % for DMEA-PZ-EG, DMEA-EDA-EG, and DMEA-MEA-EG, respectively. We can also observe that for

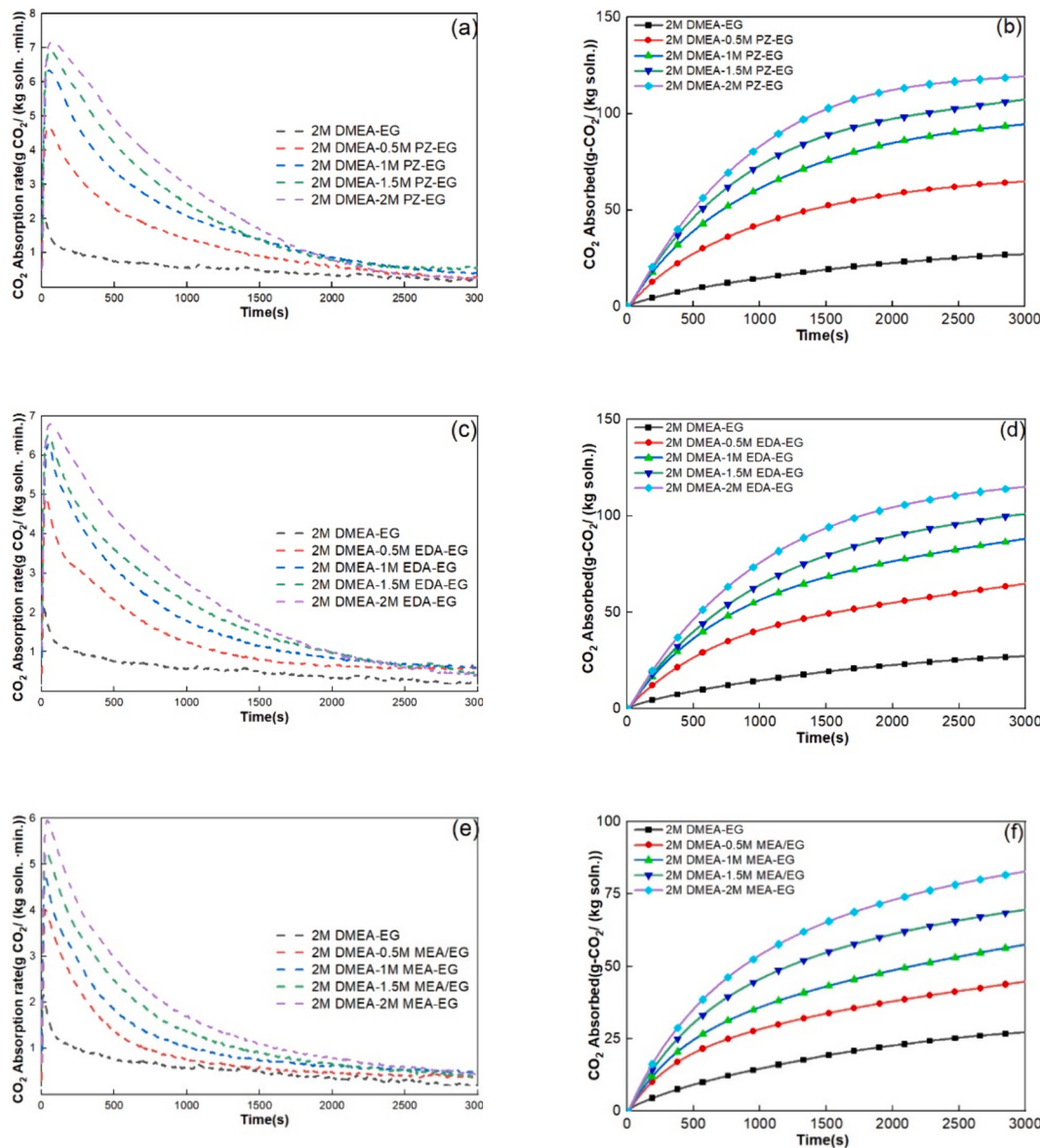


Fig. 4. CO₂ absorption profiles of DMEA-based absorbents; Left side: CO₂ absorption kinetics; Right side: CO₂ desorption kinetics. (a, b) DMEA-PZ-EG; (c, d) DMEA-EDA-EG; (e, f) DMEA-MEA-EG.

the DMEA-based absorbents with PZ and MEA as activators, their desorption performance was more similar to that of pure DMEA-EG, and increasing the temperature is less helpful for the desorption efficiency, whereas EDA does not behave similarly. In chemical structural terms, the dual primary amines present in EDA exhibit a heightened affinity for CO₂, whereas cyclic amines or a singular primary amine mitigate this solid binding effect. Consequently, DMEA-PZ and DMEA-MEA, characterized by such structural attributes, demonstrate a propensity for maintaining low-temperature regeneration ability.

Figs. S5–S7 also demonstrates that as the concentration of the activator increased from 0.5M to 2M, the regeneration efficiency of the absorbents at the same temperature decreased. Taking DMEA-PZ-EG as an example, at a desorption temperature of 343 K, the regeneration efficiency was 60.6 %, 68.4 %, 70.0 %, and 73.01 % for DMEA-2M PZ-EG, DMEA-1.5M PZ-EG, DMEA-1M PZ-EG, and DMEA-0.5M PZ-EG, respectively. As the added activators' concentration rises, the activator-CO₂ reaction could dominate the CO₂ absorption. DMEA exhibits a proclivity for proton binding with the activator as opposed to EG, which led to poor desorption performance. This indicates that excessively high concentrations of activators are not conducive to the low-temperature

regeneration of DMEA-based sorbents.

In summary, the study highlights the importance of added activators' type and concentration in determining the regeneration performance of CO₂-rich solutions. Adding an appropriate concentration of activator can enhance absorption ability while maintaining DMEA-EG absorbent for a low-temperature regeneration ability. These findings have significant implications for the design and optimization of DMEA-based absorbents, the desorption results are summarized at Table 4 below.

3.3.2. Comparison of the absorption/desorption performance of DMEA-based absorbents with 30 wt% MEA-H₂O

As discussed above, DMEA-based absorbents have demonstrated excellent desorption performance. The effective desorption process could occur at 343 K. To further confirm their desorption capabilities and potential industrial application, the DMEA-based absorbents are compared with 30 wt% aqueous MEA solutions. The desorption condition is settled as 343 K and 200 ml/min. As illustrated in Fig. 6a, at 343 K, 2M DMEA-1M PZ-EG exhibited a remarkable desorption rate, which was approximately twice that of 30 wt% MEA-H₂O (28.5 (g·CO₂/kg-soln.) vs 14.9 (g·CO₂/kg-soln.)). This suggests that in anhydrous

Table 3

CO_2 absorption loading, t_{95} and maximum absorption rate of DMEA-based absorbents, in comparison to the 30 wt% MEA-H₂O.

Solution name	$n_{\text{CO}_2}/n_{\text{amine}}$ CO_2 loading	CO_2 absorption (g-CO ₂ /kg- soln.)	Maximum r_{abs} (g-CO ₂ /(kg-soln.- min.))	t_{95} (s)
30 wt% MEA-H ₂ O (5M MEA)	0.540	116.82	7.039	1493
2M DMEA-EG	0.358	31.520	1.922	2777
2MDMEA/0.5M PZ (2-0.5)	0.591	64.879	4.703	2509
2MDMEA/1M PZ (2-1)	0.731	96.546	6.345	2413
2MDMEA/1.5M PZ (2-1.5)	0.698	107.42	6.928	2323
2MDMEA/2MPZ (2-2)	0.676	119.363	7.177	2104
2MDMEA/0.5M EDA (2-0.5)	0.589	64.781	4.955	2664
2MDMEA/1M EDA (2-1)	0.670	88.023	6.300	2580
2MDMEA/1.5M EDA (2-1.5)	0.655	100.910	6.530	2492
2MDMEA/2M EDA (2-2)	0.653	115.051	6.800	2356
2MDMEA/0.5M MEA(2-0.5)	0.410	44.700	3.994	2657
2MDMEA/1M MEA (2-1)	0.435	57.523	4.692	2623
2MDMEA/1.5M MEA(2-1.5)	0.452	69.550	5.267	2534
2MDMEA/2M MEA (2-2)	0.470	82.764	5.951	2484

condition, the product of DMEA-PZ-EG and CO₂ is much easier to decompose than MEA-CO₂ in aqueous condition.

The Fig. 6b summarizes the absorption capacity, CO₂ desorbed amount, and regeneration efficiency of 2M DMEA-EG, 2M DMEA-1M PZ-EG, 2M DMEA-1M EDA-EG, 2M DMEA-1M MEA-EG and 30 wt% MEA-H₂O. These results indicate that, at the same desorption temperature, the DMEA-based absorbents always exhibit higher regeneration efficiency than 30 wt% MEA-H₂O. Moreover, the addition of activator into 2M DMEA-EG system further improve the absorption capacity and desorption capacity significantly. MEA-H₂O demonstrated a high absorption capacity of 116 g-CO₂/(kg-soln.), but its regeneration efficiency was only 53 % at 343 K. In contrast, the CO₂ absorption capacity of 2M DMEA-1M PZ-EG is 97 g-CO₂/(kg-soln.), which is 16 % lower than that of MEA-H₂O, but its regeneration efficiency reaches to 81.5 % at 343 K, which could desorb 76 g-CO₂/(kg-soln.), 19.7 % higher than that of MEA. This means that the cyclic adsorption capacity of 2M DMEA-1M PZ-EG is much higher than the benchmark absorbent MEA-H₂O, and has great potential to be applied in industry as energy-saving absorbent for CO₂ capture.

3.4. Effect of purging gas flow rate on desorption

The desorption process involves the decomposition of the amine-CO₂ complex and then the release of CO₂ from the liquid phase to the gas phase. Various methods have been employed to enhance desorption, such as ultrasonic-assisted desorption, vacuum swing desorption, and stirring-assisted desorption [41,52,53]. These methods aim to reduce the regeneration energy penalty. This study utilized nitrogen as a purging gas during the microwave desorption process to facilitate mass transfer between the gas and liquid phases. The effect of purging gas flow rate on desorption rates and efficiency was investigated by increasing the flow rate from 100 to 250 ml/min during the dynamic desorption process, as depicted in Fig. 7. The release of CO₂ from CO₂-rich absorbents also increased with the purging gas flow rate. Taking the DMEA-PZ-EG (2:1) absorbents as an example, at a desorption

temperature of 343 K, the regeneration efficiency reached 69.95 %, 73.92 %, 80.70 %, and 81.92 % in 50 min for purging gas flow rates of 100 ml/min, 150 ml/min, 200 ml/min, and 250 ml/min, respectively.

A high flow rate purging gas brings several advantages in the desorption process, including promoting efficient removal of CO₂ bubbles from the liquid phase, enhanced mass and heat transfer, and reduced CO₂ residence time. When the purging gas flow rate reached 200 ml/min, further increases had minimal impact on desorption. Increasing the purging gas flow rate from 200 ml/min to 250 ml/min only led to a 1.9 % improvement in regeneration efficiency. Therefore, a purging gas flow rate of 200 ml/min was considered optimal for DMEA-Activator-EG absorbents in this experimental setup. The absorption-desorption circulating experiments also employed this flow rate (200 ml/min).

3.5. Kinetics and activation energy of the desorption process

To confirm that DMEA-based absorbents have high regeneration abilities, a further investigation of the desorption kinetics and enthalpy is proposed. The desorption process was conducted at six different temperatures ranged from 323 and 373 K. Hence, the first order desorption models were applied to the 2M DMEA-EG, 2M DMEA-1M PZ-EG, 2M DMEA-1M EDA-EG, and 2M DMEA-1M MEA-EG, respectively. According to previous research, the following assumptions are proposed before modelling.

1. The CO₂ desorption rate is proportional to the concentration of CO₂-rich DMEA-Activator-EG solution.
2. The CO₂ desorption process is irreversible at the initial desorption step; reaction fits the first-order kinetics equation [41].

As a result, the first-order desorption reaction equation can be written as follows [54]:

$$r = -\frac{dC_A}{dt} = kC_A \quad (3)$$

$$-In(1-x) = kt \quad (4)$$

Where k is the rate coefficient, C_A is the concentration of absorbents, t is the reaction time, and x is ratio of amine reacted with CO₂. By obtaining the data from the desorption profile, we can determine the relationship between $-In(1-x)$ and time for various DMEA-Activator-EG absorbents. After determining the rate coefficient k at different temperatures, we can apply the Arrhenius law [55]:

$$Ink = Ink_0 - \frac{E_a}{RT} \quad (5)$$

The k_0 is the pre-exponential factor (min^{-1}), E_a is the activation energy (Kj/mol) of CO₂ desorption, and R is the ideal gas constant. Relationship between k and T^{-1} of DMEA-EG, DMEA-PZ-EG, DMEA-EDA-EG and DMEA-MEA-EG are shown in Fig. 8.

The values of activation energy E_a and pre-exponential factor k_0 are concluded in Table S10. Compared to 30 wt% MEA, the activation energy of DMEA-PZ-EG is 30.32 (Kj/mol), 65 % lower than that of MEA (85–100 (Kj/mol)) [39,41,56], indicating the low energy consumption and mild condition for absorbent regeneration. The Arrhenius form of CO₂ desorption from DMEA-based absorbents are presented as follows:

$$\text{2M DMEA-EG: } k = 1396.6 * e^{\frac{-52669}{RT}} (\text{min}^{-1})$$

$$\text{2M DMEA-1M PZ-EG: } k = 1.3231 * e^{\frac{-30.318}{RT}} (\text{min}^{-1})$$

$$\text{2M DMEA-1M EDA-EG: } k = 5.3655 * e^{\frac{-35753}{RT}} (\text{min}^{-1})$$

$$\text{2M DMEA-1M MEA-EG: } k = 6.3598 * e^{\frac{-31527}{RT}} (\text{min}^{-1})$$

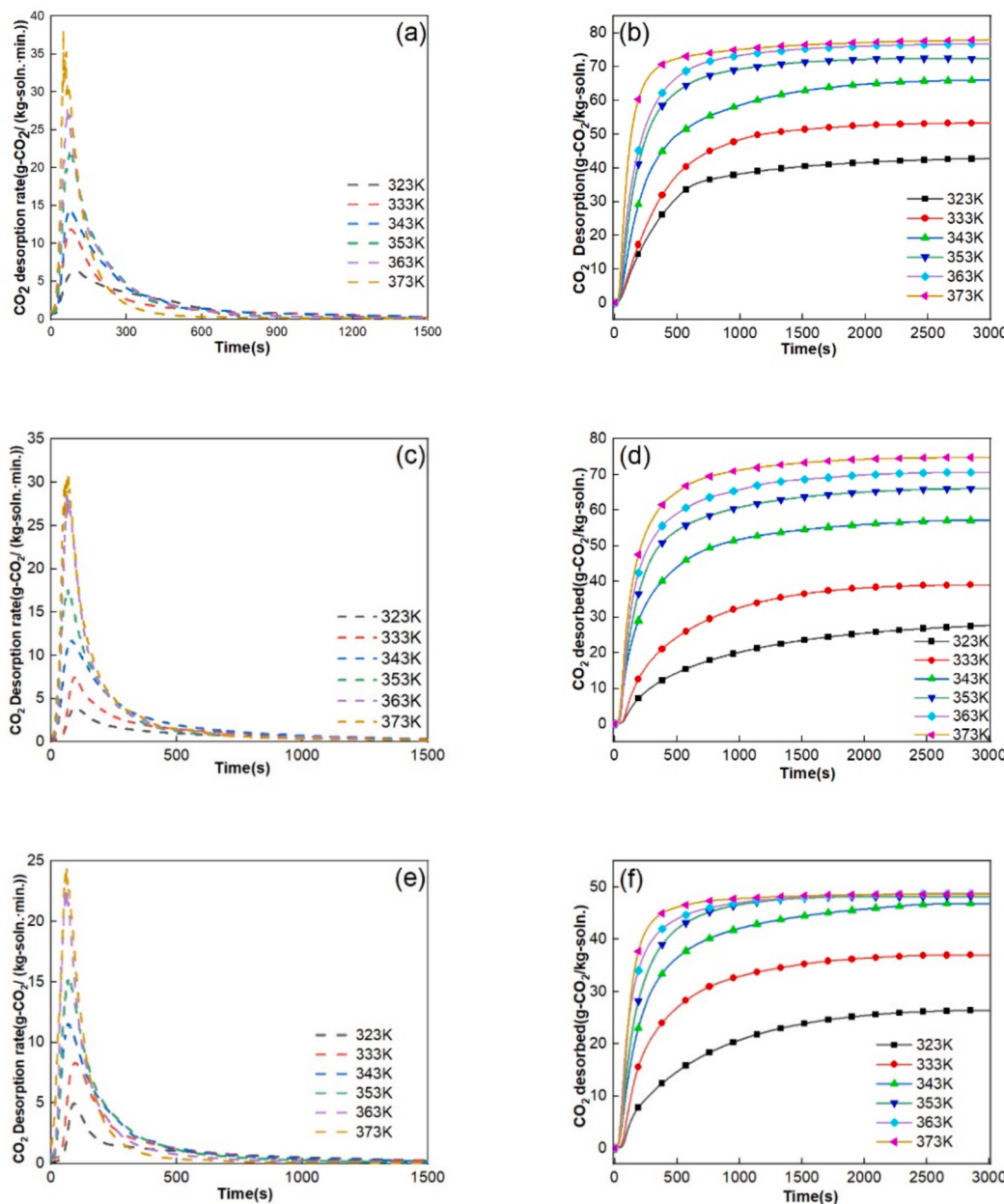


Fig. 5. CO₂ desorption profiles for DMEA-based absorbents; (a–b) CO₂ desorbed and CO₂ desorption rate of DMEA-PZ-EG; (c–d) CO₂ desorbed and CO₂ desorption rate of DMEA-EDA-EG; (e–f) CO₂ desorbed and CO₂ desorption rate of DMEA-MEA-EG; molar ratio of DMEA: Activator is 2:1; 100 ml/min nitrogen gas flow applied.

3.6. Cyclic experiment and stability of absorbents

Based on the results obtained from single absorption and regeneration steps, we selected two absorbents, 2M DMEA-1M PZ-EG and 2M DMEA-1M MEA-EG, to conduct cyclic experiments that mimic the industrial CO₂ capture process and results showed at Fig. 9. We also included a 30 %wt aqueous MEA absorbent for comparison. In each experiment cycle, CO₂ absorption was carried out at a temperature of 298 K for 50 min, followed by CO₂ desorption or solvent regeneration at 343 K for the same time. The desorption process was facilitated by purging with N₂ gas at a 200 ml/min rate.

After completing seven cycles of absorption and desorption, we analysed the performance of the absorbents. In the last cycle, the 2M DMEA-1M PZ-EG absorbent achieved a CO₂ absorption capacity of 78.98 (g-CO₂/kg-soln.), retaining approximately 80.6 % of the initial loading. Similarly, the 2M DMEA-1M MEA-EG absorbent retained 77.5 % of the initial loading in the last cycle. In contrast, the 30 %wt MEA absorbent

exhibited a significantly lower cyclic capacity. Although it initially absorbed about 110 (g-CO₂/kg-soln.), the capacity decreased to 61.68 (g-CO₂/kg-soln.) in the last cycle, representing only 54.5 % of the initial loading. This decline in cyclic capacity was much more pronounced than the DMEA-based absorbents under the same regeneration conditions (343 K, 200 ml/min N₂ purging flow).

These results demonstrate that DMEA-based absorbents exhibit superior cyclic performance compared to the 30 %wt MEA absorbent under identical regeneration conditions. This finding highlights the potential of DMEA-based absorbents for more efficient and sustainable CO₂ capture processes in industrial applications.

The effective use of absorbents in commercial applications hinges on their thermal stability. Typically, amine absorbents are subjected to heat during the regeneration process. Despite the lower desorption temperature of DMEA-based absorbents is lower, around 343 K compared to MEA's 393 K, their thermal stability warrants evaluation. The FT-IR is employed to characterize the fresh DMEA-based absorbents and the

Table 4

CO_2 desorption, t_{95}^* and maximum desorption rate of DMEA-based absorbents under different temperature in 40 min; 100 ml/min nitrogen gas flow applied.

	Desorption Temperature (K)	Maximum r_{des} (g- CO_2 /kg-soln.-min.)	CO_2 desorption (g- CO_2 /kg-soln.)	Regeneration Efficiency (%)	t_{95}^* (s)
2M DMEA- 1M PZ- EG	323	6.41	42.89	45.33 %	1772
	333	11.95	53.32	56.48 %	1309
	343	14.36	66.04	69.95 %	1464
	353	22.18	72.38	76.67 %	914
	363	28.85	76.83	81.38 %	903
	373	37.95	77.97	82.69 %	785
2MDMEA- 1M EDA-EG	323	3.88	27.64	32.41 %	2265
	333	7.48	39.16	44.34 %	1643
	343	11.67	57.14	64.95 %	1458
	353	17.56	66.03	75.06 %	1305
	363	28.46	70.62	80.26 %	1162
	373	30.78	74.76	84.96 %	968
2MDMEA- 1M MEA-EG	323	4.96	26.42	45.95 %	1876
	333	8.31	37.00	64.35 %	1583
	343	11.51	46.86	81.49 %	1465
	353	15.24	48.16	83.75 %	909
	363	22.61	48.76	84.81 %	821
	373	25.22	49.68	86.42 %	534

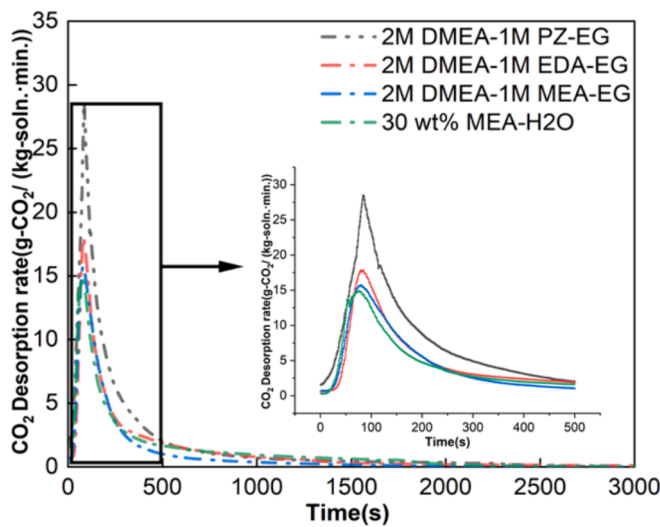


Fig. 6a. The comparison of CO_2 desorption kinetics of 2M DMEA-1M PZ-EG, 2M DMEA-1M EDA-EG, and 2M DMEA-1M MEA-EG with 30 wt% MEA- H_2O at 343 K, 200 ml/min N_2 condition.

DMEA-based absorbents after one cycle, after three cycles, and after five cycles, respectively. The FT-IR spectrum is displayed in Fig. 10.

Throughout each cycle, CO_2 absorption occurred at 298 K for 50 min, followed by CO_2 desorption or regeneration at 343 K for 50 min with N_2 gas purging. Analysis of the FTIR spectra revealed no new peaks or significant peak shifts after multiple cycles. This observation suggests that the DMEA-based absorbent exhibits excellent thermal stability. The chemical structures of DMEA-based absorbents remain unchanged, even when subjected to heat during the regeneration process.

3.7. Energy consumption of DMEA-based absorbents

3.7.1. Energy consumption measured from microwave swing process

In the CO_2 treatment process, the expensive regeneration costs limit the process's implementation [49]. Consequently, there is a need to

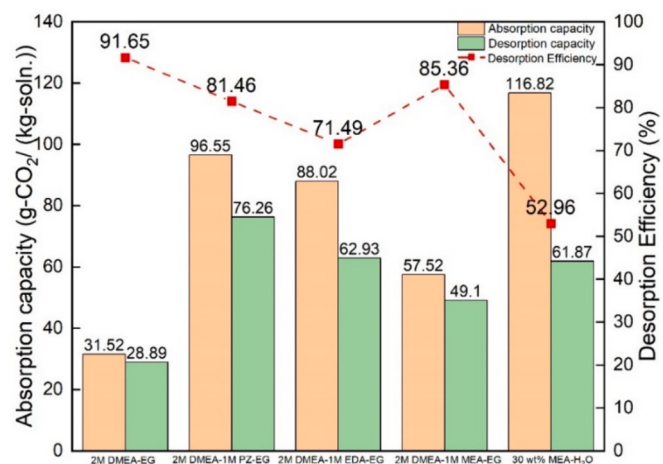


Fig. 6b. The comparison of CO_2 absorption/desorption capacity and regeneration efficiency of 2M DMEA-1M PZ-EG, 2M DMEA-1M EDA-EG, and 2M DMEA-1M MEA-EG with 30 wt% MEA- H_2O ; desorption at 343 K.

appraise the energy utilisation of DMEA-based absorbents to enable their more comprehensive industrial implementation. To address this issue, we have employed a microwave heating technique for absorbent regeneration, leveraging its advantages of instantaneous and volumetric heating while facilitating the assessment of energy consumption.

An effective absorbent for CO_2 capture should have a low energy-to-released CO_2 ratio, referred to as EC (Energy per CO_2 in Kj/mol), as defined by Eq. (1). We generated dynamic EC graphs for absorbents with various activator concentrations and different purging gas flow rates separately. In Fig. 11 (a), (c), and (e), the purging gas flow was maintained at 100 ml/min. In contrast, in Fig. 11 (d), (e), and (f), the activators (PZ, EDA, and MEA) concentration was kept at 1M. All energy consumptions were measured at the absorption-desorption circulating temperature of 343 K.

The EC values followed a concave curve with an optimum (minimum) observed, as shown in Fig. 11. During the initial temperature-increasing stage, increasing the absorbents from room temperature (298 K) to the desired temperature (343 K) consumed large amounts of energy with little CO_2 released. As the temperature reaches the specified value shortly, the energy input decreases, and a high quantity of stripped CO_2 reduces EC to a minimum. Subsequently, as energy was continuously supplied to the solution with less and less CO_2 being stripped, the EC value started to rise again.

We examined the influence of activator concentration and purging gas flow rate on energy consumption (EC) during CO_2 desorption. Our findings demonstrate that high-velocity purging gas effectively reduces the energy penalty for all DMEA-based absorbents, resulting in lower EC values during the regeneration cycle experiments. Comparatively, DMEA-PZ-EG and DMEA-EDA-EG exhibit relatively low EC values, whereas DMEA-MEA-EG shows higher EC values. The minimum EC values observed for DMEA-PZ-EG and DMEA-EDA-EG are approximately 500–600 Kj/mole, while DMEA-MEA-EG can reach 700–800 Kj/mole values. Furthermore, the activator concentration notably impacts the minimum EC values, displaying a downward trend as concentration increases. This relationship can be attributed to the substantial increase in CO_2 release from the absorbents due to the addition of the activators, which surpasses the corresponding increase in energy consumption.

From the desorption method perspective, microwave heating operates based on the ability of molecules with a dipole moment to absorb microwave energy and convert it into heat. The dielectric constant determines a substance's capacity to absorb microwaves. Among the tested chemicals, PZ and EG exhibits the lowest and highest dielectric constant (37.72 for MEA, 17.18 for DMEA, 4.52 for PZ, 13.3 for EDA, 39.84 for EG, and 78.5 for water) [57]. Consequently, when we employ

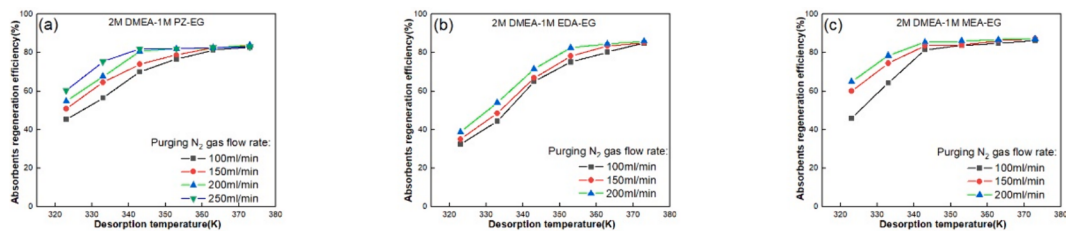


Fig. 7. The summary of CO₂ desorption efficiency of DMEA-based absorbents with different nitrogen gas flow under different temperature; (a) DMEA-PZ-EG (2:1); (b) DMEA-EDA-EG (2:1); (c) DMEA-MEA-EG (2:1).

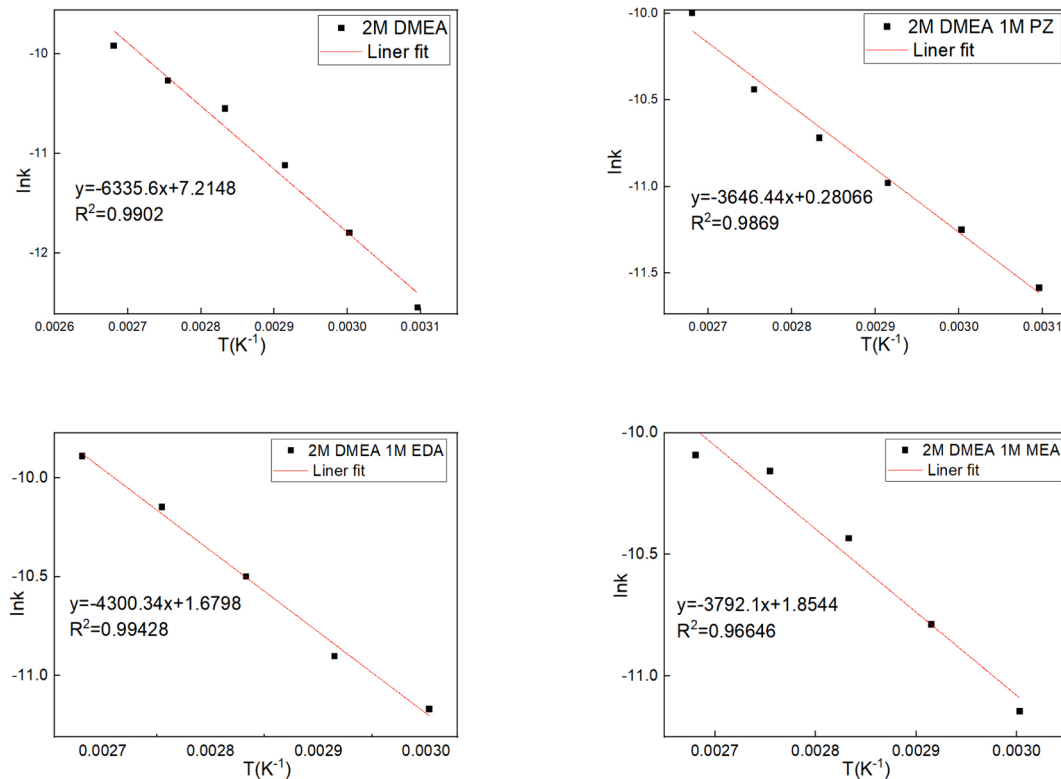


Fig. 8. Arrhenius plots for desorption of DMEA-based absorbents, including DMEA-EG, DMEA-PZ-EG, DMEA-EDA-EG and DMEA-MEA-EG with acceptable R² values.

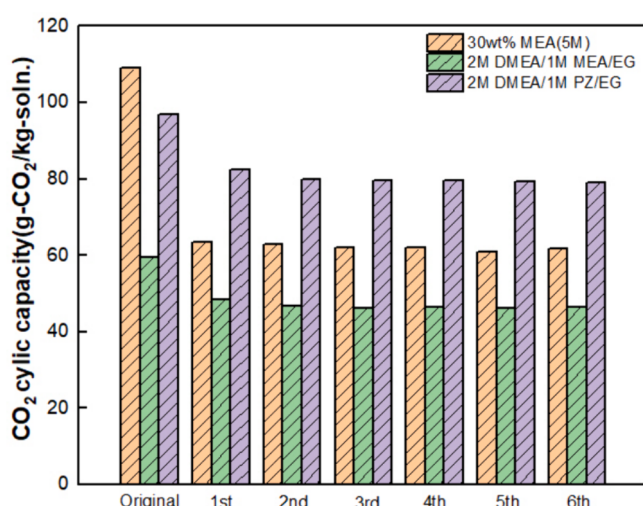


Fig. 9. Cyclic capacity of 2M DMEA-1M PZ-EG and 2M DMEA-1M MEA-EG, compared with 30 wt% MEA-H₂O. (Desorption condition: 343 K, 200 ml/min N₂ purging flow).

microwaves to heat DMEA-based absorbents to the same temperature, PZ absorbs the least amount of microwave energy. In practical terms, this means that the absorbent containing PZ as the activator requires the least amount of microwave energy input. In contrast, most of the microwave energy is absorbed by EG, causing the entire system to heat up [30]. Among the three mixtures, DMEA-PZ-EG is the most suited DMEA-based absorbent for desorption through microwave treatment due to the low dielectric constant of PZ. It should be noted that water, with its high dielectric constant value, is not a favourable solvent in the microwave desorption process [31].

Moreover, determining the steady-state EC values of DMEA-based absorbents is crucial for comparison with previous literature [31,33]. During desorption, more than 90 % of CO₂ is released in the first 20 min. Hence, the microwave energy consumption and CO₂ released in the first 20 min of the desorption process at a desorption temperature of 343 K is taken to calculate the steady-state EC values, the calculation method has been described in the literature [32]. The results of the study comparing aqueous and non-aqueous MEA absorbents are presented in Table 5. Among the listed absorbents, DMEA-PZ-EG has the lowest EC, which is 77.5 % lower than MEA-H₂O. Furthermore, all non-aqueous absorbents exhibited low EC values compared to aqueous absorbents. Therefore, from the perspective of microwave regeneration, microwave

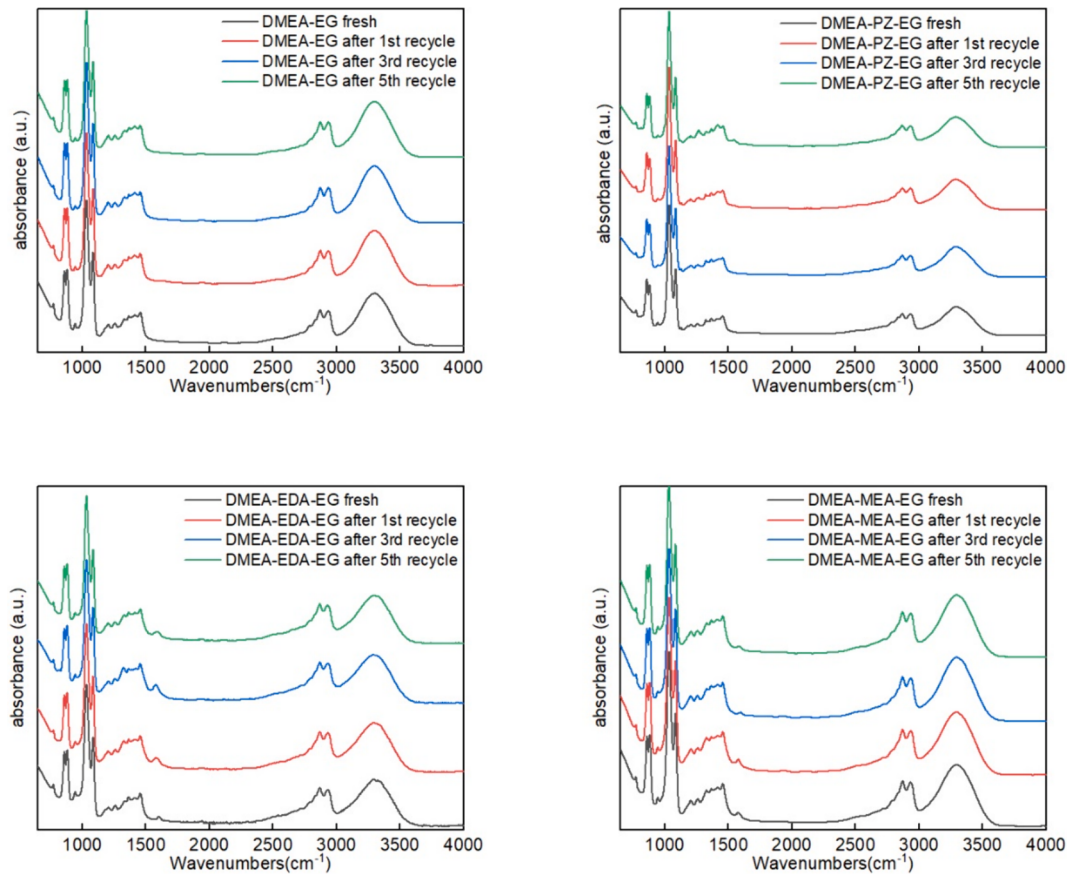


Fig. 10. FT-IR spectrum of recycled DMEA-based absorbents. From top left to right: 2M DMEA-EG and 2M DMEA-1M PZ-EG. From bottom left to right: 2M DMEA-1M EDA-EG and 2M DMEA-1M MEA-EG.

regeneration is not suitable for aqueous absorbents.

However, it should be noted that the microwave energies measured in this study are specific to the experimental setup used and cannot be directly compared to values from other literature [2]. The microwave desorption energy measured for small samples of 5 g in this work is known to overestimate the energy consumption required to strip CO₂, as the reactor was only partially heated by a microwave heater [59]; resulting in a relatively high heat loss. All these energy losses were not solely consumed for CO₂ desorption but are included in the energy consumption measured for CO₂ desorption. However, the data listed in Table 5 can be used to compare energy efficiency for different absorbents, as the energy loss for all the experiments is the same. To further confirm the energy saving of the developed absorbents, energy consumption is also calculated-based on thermodynamics functions and following the ideal regeneration process.

3.7.2. Energy consumption calculated by thermodynamics functions

The regeneration energy (Q) consists of three parts: the reaction heat of desorption (Q_r), the latent heat of vaporization (Q_v), and the sensible heat (Q_s). The calculation formulas are shown below:

$$Q = Q_s + Q_r + Q_v \quad (6)$$

$$Q_s = \frac{C_p m_L \Delta T}{m_{CO_2}} = \frac{C_p \Delta T}{c_{ab} x M_{CO_2}} \quad (7)$$

$$Q_r = \frac{n_{CO_2} \Delta H}{m_{CO_2}} = \frac{\Delta H}{M_{CO_2}} \quad (8)$$

$$Q_v = \frac{n_w \Delta H_{H_2O}}{m_{CO_2}} = \frac{n_w \Delta H_{H_2O}}{n_{CO_2} M_{CO_2}} \quad (9)$$

As seen at Eq. (6), to calculate the sensible heat (Q_s), the specific heat capacity (C_p) of the DMEA-based absorbents is needed for the calculation. The average heat capacities of DMEA/PZ/EG, DMEA/EDA/EG, and DMEA/MEA/EG is 2.75, 2.82, and 2.78 (K/(Kg*K)), and the results of sensible heat are presented at Table 6. The specific heat capacity of the mixture is calculated from the sum of the specific heat capacities of the molar ratios of each component. The reaction heat (Q_r) during CO₂ desorption process is measured by DSC and the results are presented in Fig. S12. The calculated reaction heat for DMEA-PZ-EG, DMEA-EDA-EG, DMEA-MEA-EG, and DMEA-EG are 0.573, 0.495, 0.447, and 0.652 KJ/g CO₂, respectively. To ensure that the measured reaction heat is accurate, the reaction heat of 30 wt% aqueous MEA is measured first, and the value is 1.892 KJ/g CO₂, which is consistent with the previous research (1.818–2.5 KJ/g CO₂) [5]. Vaporization latent heat of DMEA-based absorbents is also called phase change heat. As the desorption temperature of 343 K is significantly lower than the vaporization temperature of each component in DMEA-based absorbents, the heat loss from vaporization is negligible.

In Table 6, the regeneration energy consumption value of 30 wt% MEA aqueous absorbent is 3.84 KJ/g CO₂. The Q_{total} of DMEA-PZ-EG developed in this study is 1.86 KJ/g CO₂, which is about 51.56 % lower than that of MEA-H₂O. For DMEA-based absorbents, the values of $Q_{sensibleheat}$ are much lower than that of MEA-H₂O. This could be attributed to the low heat capacity of solvent (EG). Similarly, the value of $Q_{reactionheat}$ (0.573 KJ/g CO₂) for DMEA-PZ-EG was also lower than that for MEA-H₂O (1.795 KJ/g CO₂). It could be attributed to the instability of EG alkyl-carbonates.

In conclusion, our developed DMEA-based absorbents' energy savings from microwave measurement and thermodynamic calculation agreed well. The results consistently showed that non-aqueous DMEA-

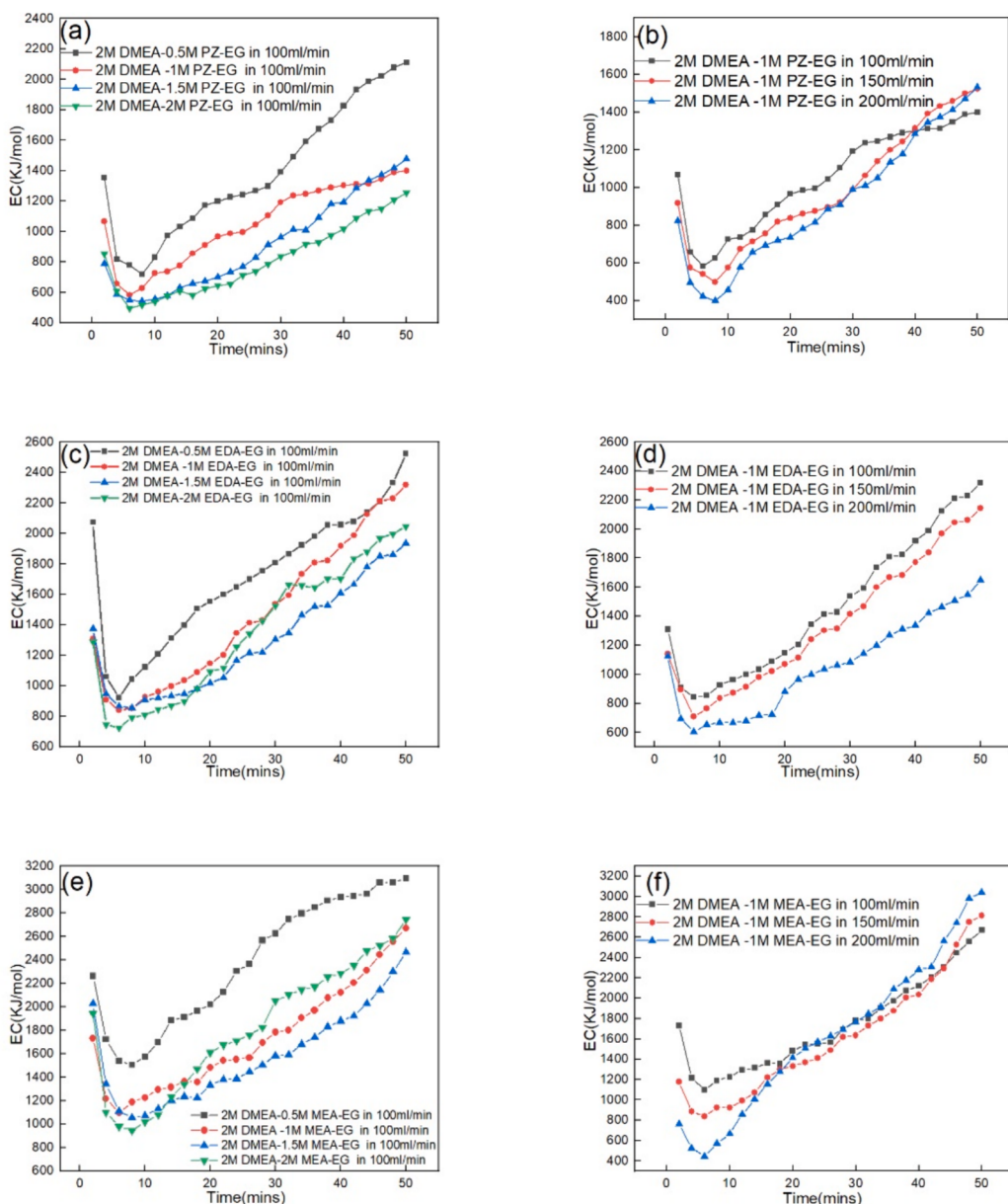


Fig. 11. Dynamic EC graphs for different concentrations of activators and purging gas flow rate of DMEA-based absorbents; (a), (b) DMEA-PZ-EG absorbents; (c), (d) DMEA-EDA-EG absorbents; (e), (f) DMEA-MEA-EG absorbents.

Table 5
Results of steady-state energy consumption about cycling CO_2 capture experiments.

Absorbents	CO_2 absorption capacity (mole)	Energy (J)	EC(Kj/mol)
2M DMEA-1M PZ-EG	0.00818	6176	755
2M DMEA-1M MEA-EG	0.00511	6794	1329
30 wt% MEA-H ₂ O [58]	0.0045	15,129	3362
30 wt% MEA-DEGMEE [58]	0.0052	4890	929
40 wt% MEA-EG/PrOH [58]	0.0060	10,193	1700

based absorbents have much lower energy requirements. Specifically, when considering microwave regeneration, DMEA-PZ-EG was found to be more efficient compared to MEA-H₂O. These findings suggest that DMEA-PZ-EG has great potential as an energy-saving absorbent for CO_2

Table 6
Regeneration energy estimated by thermodynamics equations and process simulation.

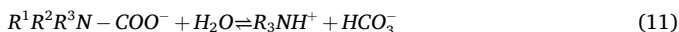
	DMEA-PZ-EG (2:1)	DMEA-EDA-EG (2:1)	DMEA-EDA-EG (2:1)	DMEA-EG (2M)	30 wt% MEA*
$C_p(\text{kJ}/(\text{kg}^*\text{K}))$	2.75	2.82	2.78	3.95	—
$Q_{\text{sensibleheat}}$	1.287	1.419	2.09	3.63	1.961
$Q_{\text{reactionheat}}$	0.573	0.495	0.447	0.652	1.795
$Q_{\text{vaporizationheat}}$	0	0	0	0	0.068
Q_{total}	1.860	1.914	2.537	4.282	3.84

* is the results from literature which calculated in the same method.

capture and regeneration.

3.8. Reaction mechanism of CO_2 capture in DMEA based absorbents

The reaction mechanism of aqueous tertiary amines, such as DMEA, has been extensively studied and reported in the literature. The CO_2 reaction with tertiary amine aqueous solutions involves the formation of carbamic acid intermediates and carbonates [59,60], where tertiary amine reacts with CO_2 to form an unstable carbamate (reaction (10)), then undergoes proton transfer with water to form bicarbonate ions (reaction (11)). The tertiary amines have a theoretical capture capacity of one mole of CO_2 per mole of amine.



Theoretical considerations suggest that, under anhydrous conditions, the reaction mechanism of tertiary amines with CO_2 is not clear. Some researchers suggested that non-aqueous tertiary amines cannot react with CO_2 [61]. This is due to the lack of a hydrogen atom attached to the nitrogen atom in tertiary amines, which is necessary for the direct formation of carbamates. However, the exceptional CO_2 absorption performance observed in this study suggests a different reaction mechanism in the tertiary amine DMEA and EG mixture. To further elucidate this mechanism, qualitative analyses were conducted using FT-IR and NMR spectroscopy [62].

The ATR FT-IR was used to analyses the reaction products of the DMEA-based absorbents with CO_2 for 0, 3, 5, 10, 20, 30, 40 and 50 min to identify the reaction mechanism. Additionally, the ^{13}C NMR spectra of fresh and CO_2 -saturated DMEA-based absorbents are taken to verify the reaction products of DMEA- CO_2 . The FT-IR spectrum of the DMEA-based absorbents during CO_2 absorption is shown in Fig. 12, and the 1D NMR spectrum is shown in Figs. S14–S21.

For DMEA-EG binary absorbents, after CO_2 absorption, the FT-IR spectra (Fig. 12 (a)) suggest two medium peaks and two minor peaks appeared in the region of 800–1700 cm^{-1} . The medium peaks at 1294 and 1640 cm^{-1} indicated the C—O and C=O stretching vibration, which means the formation of EG alkyl carbonate(R—O—COO[−]). Since DMEA is a tertiary amine, there are no N—H characteristic peaks appearing at 1500–1600 cm^{-1} region (N—H rocking). The two minor peaks at 992 and 827 cm^{-1} may be from C—N bending or torsions. The ^{13}C NMR results also confirmed the presence of alkyl carbonate at 162.04 and 159.34 ppm, indicating that the EG is deprotonated and reacts with CO_2 .

With the addition of the activators (PZ/EDA/MEA), the reaction becomes much more complex. The FT-IR spectrum of DMEA-PZ-EG under different CO_2 loading is shown in Fig. 12 (b). Compared to the DMEA-EG, additional peaks appeared or shifted because of carbamate and bicarbonate formation, the protonation of the amine group, and the dissolution of molecular CO_2 . Different from the IR spectrum of the fresh sample, seven new peaks appear at 814, 997, 1256, 1284, 1410, 1549, and 1636 cm^{-1} after CO_2 absorption. The 1549 and 1410 cm^{-1} peaks were assigned to C=O asymmetric and symmetric stretching, which belongs to PZ-carbamate. The strong peaks at 1256 cm^{-1} are likely assigned to C—N stretching. New peaks observed at 1636 and 1284 cm^{-1} correspond to the C—O and C=O stretching vibrations, respectively, similar to those observed in the DMEA-EG absorbents. The ^{13}C NMR spectrum confirmed the presence of PZ-bi-carbamate and PZ-carbamate at 161.34 and 159.39 ppm, and EG alkyl carbonate peak appears at 163.10 and 162.47 ppm [12,41,42]. The observed reaction sequence indicates that the active sites of PZ have been depleted, resulting in EG taking over as the primary component for absorbing CO_2 . This dynamic shift highlights the progression of the reaction and the transition from PZ to EG in terms of their roles in CO_2 absorption.

In the case of the DMEA-EDA-EG solution, similar IR and NMR

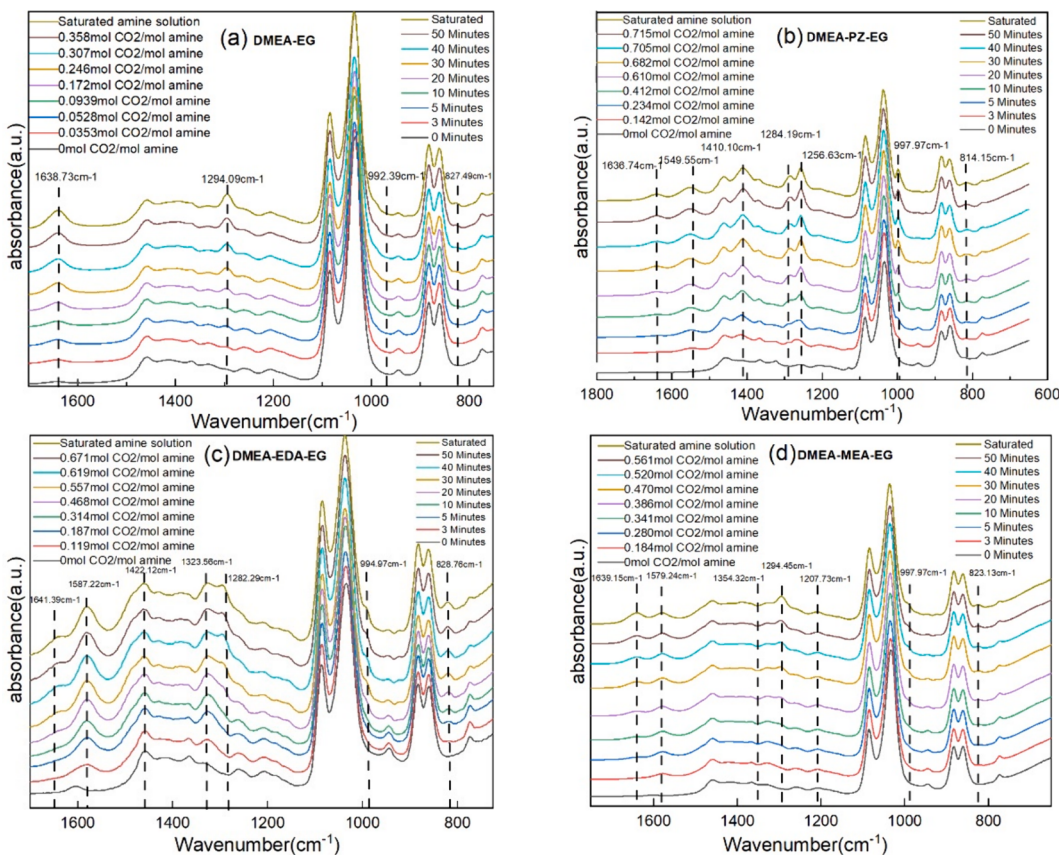


Fig. 12. ATR-FTIR spectrum of DMEA-based absorbents (0 min) and after bubbling CO_2 at 3, 5, 10, 20, 30, 40 and 50 min; (a) DMEA-EG; (b)DMEA-PZ-EG; (c)DMEA-EDA-EG; (d)DMEA-MEA-EG.

spectra were observed. However, after CO_2 absorption, seven new peaks appeared in the IR spectrum at 828, 994, 1282, 1323, 1422, 1567, and 1641 cm^{-1} . The peaks at 1567 and 1422 cm^{-1} were assigned to the asymmetric and symmetric stretching of $\text{C}=\text{O}$ bonds, while the peak at 1282 cm^{-1} was attributed to the stretching of $\text{C}-\text{N}$ bonds. These four IR peaks are characteristic of EDA-carbamate. Furthermore, two new peaks were observed at 1641 and 1323 cm^{-1} , representing $\text{C}-\text{O}$ and $\text{C}=\text{O}$ stretching vibrations, which are similar to those observed in the DMEA/EG absorbents. A comprehensive overview of all signal peaks can be found in Fig. 12 (c). The presence of EDA-carbamate was confirmed by the ^{13}C NMR spectrum, showing a peak at 158.96 ppm . Furthermore, the presence of EG alkyl carbonate was identified with peaks at 161.28 and 164.15 ppm .

In the case of the DMEA-MEA-EG solution, the ^{13}C NMR spectra confirmed the presence of MEA-carbamate at 159.36 ppm and EG alkyl carbonate at 161.70 and 164.61 ppm . The location of IR spectrum peaks in this solution is similar to that of DMEA-PZ-EG and DMEA-EDA-EG, with slight shifts. More details can be found in Fig. 12 (d).

2D NMR analysis using HMQC (Heteronuclear Multiple Quantum Coherence) is employed to investigate the formation of alkyl carbonate and the protonation of DMEA. In the presented analysis, Fig. 13 exhibits a partial HMQC 2D NMR spectrum of CO_2 -loaded DMEA-PZ-EG. The choice of DMEA-PZ-EG is based on its strong NMR signal peak, which facilitates effective 2D NMR analysis.

In Fig. 13 (a), the spectrum reveals carbon signals at 162 – 163 ppm , corresponding to carbonate species. These signals demonstrate long-range correlation with hydrogen α of EG at 3.5 ppm . This correlation implies the involvement of alkyl carbonate formation, where the product interacts with the hydroxyl groups of EG.

Fig. 13 (b) indicates a correlation between hydrogen and carbon of protonated DMEA. The hydrogen α located at 2.91 ppm , have long-range correlation with carbon **1** and **2** on DMEA, and another long-range correlation signal showed at hydrogen **b** at 2.87 ppm with carbon **1** and **3**. This correlation confirms that the bubbling of CO_2 in the DMEA-PZ-EG solution led to the protonation of DMEA, resulting in an up-field shift of these carbon signals. However, the other signals observed between 3.00 and 3.10 ppm , which emerged following the protonation of DMEA, could not be definitively assigned at this stage.

Based on the characterization results discussed in the above sections, we have proposed the CO_2 absorption mechanism of DMEA-based absorbents based on the FT-IR and NMR spectra measured.

For the DMEA-EG binary absorbent, the reaction involves the deprotonation of EG, followed by its reaction with CO_2 to form alkyl carbonate. However, due to the weak affinity between EG and CO_2 , this reaction proceeds very slowly. The tertiary amine group in DMEA lacks a proton and cannot generate DMEA carbamate. Additionally, in the absence of water in the non-aqueous environment, CO_2 cannot undergo hydration to form $\text{HCO}_3^-/\text{CO}_3^{2-}$.

In the case of the DMEA-Activator-EG ternary absorbent, along with alkyl carbonate formation, carbamate is also generated. When CO_2 is absorbed in the presence of an activator (PZ, EDA, or MEA), the initial reaction occurs between CO_2 and the amine group of the activator. This reaction is rapid due to the strong affinity between the activator and CO_2 . Therefore, adding PZ, EDA, or MEA significantly increases the CO_2 absorption capacity from $31.53\text{ (g-CO}_2/\text{kg-soln.)}$ to 96.54 , 88.02 and $57.52\text{ (g-CO}_2/\text{kg-soln.)}$. The maximum absorption rate also increases from $1.92\text{ (g-CO}_2/(\text{kg-soln.}\cdot\text{min.}))$ to 6.34 , 6.30 and $4.69\text{ (g-CO}_2/(\text{kg-soln.}\cdot\text{min.}))$, respectively. The tertiary amine DMEA, with its strong nucleophilicity, acts as a proton transfer and receiver, enhancing both the absorption rate and capacity of CO_2 . After absorption, CO_2 is primarily bonded on EG, and the $\text{C}-\text{O}$ bond in the alkyl carbonate is much weaker than the $\text{C}-\text{N}$ bond in the carbamate, allowing for easy regeneration and recycling under mild conditions. According to previous research, the decomposition temperature of EG alkyl carbonate is around 323 K , much lower than that of MEA carbamate (393 K) [63]. Besides, from the molecular dynamics point of view, adding activators

improves the solubility of DMEA-EG absorbents, allowing them to dissolve more CO_2 .

In the protonation process of DMEA, the DMEA accept the proton through the hydrogen bonds formed between DMEA zwitterion and EG. To confirm this mechanism, a set of structures with the ternary combination of EG, CO_2 and the DMEA (organic base) were computed as shown in Fig. 14 (b) below. The CO_2 reacts with DMEA to form an intermediate zwitterion, then this intermediate zwitterion interacts with EG (species 2 in Fig. 14 (b)). The EG carbonate is formed by the reaction of one of the hydroxyl groups of EG with CO_2 and the DMEA acting as an ancillary. Although the hydroxyl group itself is not basic enough to react with CO_2 , the base (DMEA) may activate it after formation of an intermolecular hydrogen bond between the base and the glycerol (species 1 in Fig. 14 (b)) [39,64]. The existence of the intermolecular hydrogen bond was confirmed both by its interaction enthalpy ($\Delta E = -15.0576\text{ KJ/mol}$) and by the donor-acceptor distance (1.917 \AA). This hydrogen bond activates EG to perform a nucleophilic attack on the acid carbon of CO_2 , which occurs accompanied by a concerted proton transfer from the EG to the base (species 3 in Fig. 14 (b)). Depending on the base strength, the proton can be donated back to the carbonate, forming organic bi-carbonate (species 4 in Fig. 14 (b)). Similar mechanism is also conducted in previous research [64]. The possible reaction mechanisms and routes are comprehensively investigated and summarized in Fig. 14.

4. Conclusion and outlook

This study introduces a robust and efficient activator screening methodology grounded in MD simulations. The effectiveness of non-aqueous absorbents in capturing CO_2 is intrinsically linked to the solubility of amine- CO_2 products in organic solvents. The proposed screening approach considerably streamlines experimental efforts and serves as a guide for innovating new CO_2 absorbents designs. This is corroborated by DFT calculations, which affirm that including activators effectively reduces the solvation free energy of DMEA-EG, enabling more significant CO_2 dissolution in the absorbent.

Our comprehensive investigation leverages both theoretical and experimental work, culminating in developing a novel non-aqueous CO_2 absorbent with a low regeneration energy requirement. The non-aqueous DMEA-based absorbents demonstrate remarkable reversibility in CO_2 uptake under mild conditions (343 K). We have thoroughly assessed aspects such as absorption and desorption performance, cyclic stability, energy consumption, and the underlying mechanisms of DMEA-based absorbents. Within the realm of DMEA-EG binary absorbents, adding the activators significantly augments absorption rates and capacities. Among different developed DMEA-based absorbents, 2M DMEA 1M PZ EG is the top performer, exhibiting a regeneration efficiency 1.31 times higher than aqueous MEA despite with a lower molar fraction (2M DMEA 1M PZ versus 5M MEA). The regeneration energy consumption for DMEA-PZ-EG stands at a mere 1.86 KJ/g CO_2 , in contrast to the 3.84 KJ/g CO_2 required by 30 wt% aqueous MEA, resulting in a remarkable 51.56 % reduction.

This novel DMEA-based absorbent demonstrates exemplary recyclability and thermal stability, as evidenced by thorough TGA analyser and absorption-desorption recycling experiments. Through an integrated approach involving IR and NMR spectroscopy, we unveil the intricate absorption mechanism of DMEA-based absorbents. CO_2 initially binds with activators during absorption, giving rise to zwitterionic compounds, while DMEA functions as a proton acceptor to yield DMEA^+ . Simultaneously, CO_2 reacts with EG in a deprotonation process, forming EG alkyl carbonate, which governs the CO_2 absorption dynamics. The corroborative 2D NMR spectrum confirms the presence of DMEA^+ and EG alkyl carbonate. Importantly, this novel CO_2 absorption mechanism fosters a weak interaction between CO_2 and the absorbent, thereby substantially reducing energy consumption. Furthermore, the desorption activation energy for DMEA-PZ-EG stands at a mere 30.32 KJ/mole , further attesting to the weak interaction

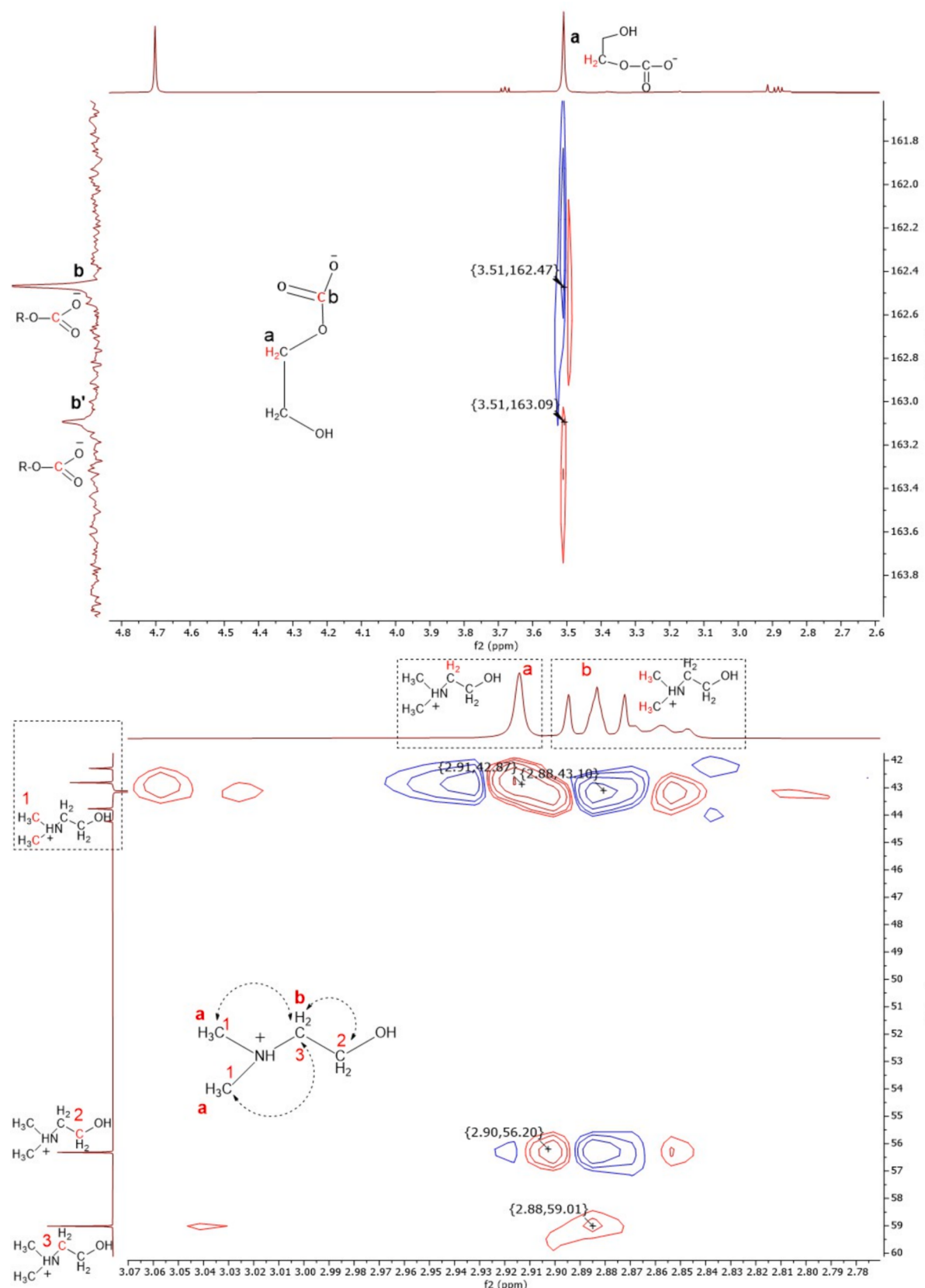


Fig. 13. (a) Partial HMBC 2D NMR spectrum of saturated DMEA-PZ-EG showing the correlations of carbonate species. (b) Partial HMBC 2D NMR spectrum of saturated DMEA-PZ-EG showing the C-H correlations of protonated DMEA.

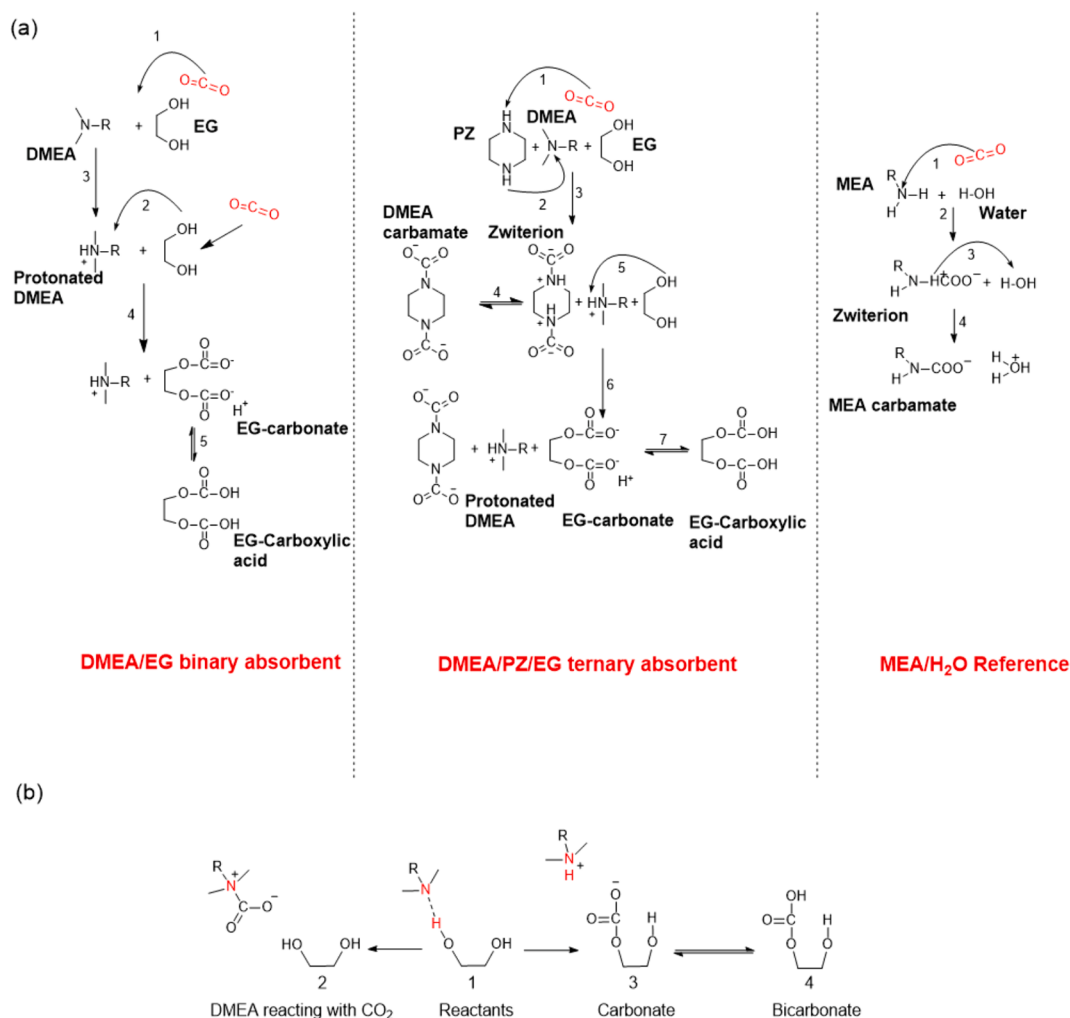


Fig. 14. (a) The reaction routes between DMEA-EG with CO₂, DMEA-PZ-EG with CO₂ and MEA-H₂O as reference. (b) CO₂ capture by the DMEA-based absorbents and the possible products 2, 3 and 4.

between CO₂ and the amine. Collectively, the DMEA-based absorbents open new avenues for advancing next-generation amine absorbents, poised for commercial applications in CO₂ capture.

Single-atom absorbents have attracted much attention recently because of their super low CO₂ regeneration energy consumption. It combines the advantages of single-atom catalysts and nanofluids, which are defined as single-atom solutions. In this novel single-atom solution, nickel, copper, or other metal atoms are dispersed uniformly in the solvent. Using strong catalysis of a single metal atom, the thermoelectric effect of solvents will be produced, which enhances the CO₂ desorption rate by lowering the desorption energy barrier. Finally, due to these traits, near zero energy consumption CO₂ capture will be realized since the substantial waste heat below 373 K will be easily harvested by the single atom solution. According to the Chenyang et al. study [65], the energy consumption of copper and boron based single-atom CO₂ capture solutions were assessed as 1.65 Kj/g CO₂ and 0.97 Kj/g CO₂, which are 56.58 % and 74.47 % lower than the MEA amine system [65–68]. The critical components of this solution are the single-atom catalyst and the amine absorbents. Current studies often use conventional monoethanolamine (MEA) as the amine absorbent in single-atom CO₂ capture solutions. However, combining advanced non-aqueous amine absorbents with single-atom catalysts can further reduce energy consumption. For example, combining the DMEA-based absorbent developed in this study with a single-atom catalyst could lower energy use and improve regeneration efficiency. This DMEA-based single-atom CO₂ capture

solution has significant potential to replace current CO₂ absorbents.

Declaration of competing interest

The authors declare that they have no known competing financial interests or personal relationships that could have appeared to influence the work reported in this paper.

Data availability

Data will be made available on request.

Acknowledgement

This work was supported by Engineering and Physical Sciences Research Council (EP/V041665/1, EP/W027593/1).

Appendix A. Supplementary material

Supplementary data to this article can be found online at <https://doi.org/10.1016/j.seppur.2024.128996>.

References

- [1] A. Lee, et al., Policies and incentives developments in CO₂ capture and storage technology: a focused survey by the CO₂ capture project, Carbon Dioxide Capture

- Storage Deep Geol Form. - Results from CO 1 (2005) 17–35, <https://doi.org/10.1016/B978-008044570-0/50086-6>.
- [2] G. Lu, Z. Wang, U.H. Bhatti, X. Fan, Recent progress in carbon dioxide capture technologies: a review, 1(1) (2023), doi: 10.18686/cest.v1i1.32.
 - [3] UNFCCC, CMA3 - Glasgow Climate Pact, Cma3, 2 (2021) 1–11.
 - [4] F. Yang et al., Means of the cosolvent effect, (2018) 2328–2336, doi: 10.1039/c8gc00283e.
 - [5] W. Tian, et al., Nonaqueous MEA/PEG200 absorbent with high efficiency and low energy consumption for CO2 capture, Ind. Eng. Chem. Res. 60 (10) (2021) 3871–3880, <https://doi.org/10.1021/acs.iecr.0c05294>.
 - [6] E. Kruszczak, H. Kierzkowska-Pawlak, CO2 capture by absorption in activated aqueous solutions of N, N-diethyllethanolamine, Ecol. Chem. Eng. S 24 (2) (2017) 239–248, <https://doi.org/10.1515/echs-2017-0016>.
 - [7] S. Liu, H. Gao, C. He, Z. Liang, Experimental evaluation of highly efficient primary and secondary amines with lower energy by a novel method for post-combustion CO2 capture, Appl. Energy 233–234 (September 2018) (2019) 443–452, <https://doi.org/10.1016/j.apenergy.2018.10.031>.
 - [8] K. Fu, W. Rongwong, Z. Liang, Y. Na, R. Idem, P. Tontiwachwuthikul, Experimental analyses of mass transfer and heat transfer of post-combustion CO2 absorption using hybrid solvent MEA–MeOH in an absorber, Chem. Eng. J. 260 (2015) 11–19, <https://doi.org/10.1016/J.CEJ.2014.08.064>.
 - [9] S. Chen, S. Chen, Y. Zhang, L. Qin, C. Guo, J. Chen, Species distribution of CO2 absorption/desorption in aqueous and non-aqueous N-ethylmonoethanolamine solutions, Int. J. Greenh. Gas Control 47 (2016) 151–158, <https://doi.org/10.1016/J.IJGGC.2016.01.046>.
 - [10] C. Guo, S. Chen, Y. Zhang, G. Wang, Solubility of CO2 in nonaqueous absorption system of 2-(2-aminoethylamine)ethanol + benzyl alcohol, J. Chem. Eng. Data 59 (6) (2014) 1796–1801, https://doi.org/10.1021/JE401028G/ASSET/IMAGES/MEDIUM/JE-2013-01028G_0010.GIF.
 - [11] I.I. Alkhathib, L.M.C. Pereira, A. Alhajaj, L.F. Vega, Performance of non-aqueous amine hybrid solvents mixtures for CO2 capture: a study using a molecular-based model, J. CO2 Util. 35 (2020) 126–144, <https://doi.org/10.1016/J.JCOU.2019.09.010>.
 - [12] J. Tan, H. Shao, J. Xu, L. Du, G. Luo, Mixture absorption system of monoethanolamine–triethylene glycol for CO2 capture, Ind. Eng. Chem. Res. 50 (7) (2011) 3966–3976, <https://doi.org/10.1021/IE101810A>.
 - [13] J. Li, C. You, L. Chen, Y. Ye, Z. Qi, K. Sundmacher, Dynamics of CO2 absorption and desorption processes in alkanolamine with cosolvent polyethylene glycol, Ind. Eng. Chem. Res. 51 (37) (2012) 12081–12088, <https://doi.org/10.1021/IE301164Y>.
 - [14] C.H. Yu, T.W. Wu, C.S. Tan, CO2 capture by piperazine mixed with non-aqueous solvent diethylene glycol in a rotating packed bed, Int. J. Greenh. Gas Control 19 (2013) 503–509, <https://doi.org/10.1016/J.IJGGC.2013.10.014>.
 - [15] C. Zheng, J. Tan, Y.J. Wang, G.S. Luo, CO2 solubility in a mixture absorption system of 2-amino-2-methyl-1-propanol with glycol, Ind. Eng. Chem. Res. 51 (34) (2012) 11236–11244, <https://doi.org/10.1021/IE3007165>.
 - [16] T. Ping, Y. Dong, S. Shen, Energy-efficient CO2 capture using nonaqueous absorbents of secondary alkanolamines with a 2-butoxyethanol cosolvent, ACS Sustain. Chem. Eng. 8 (49) (2020) 18071–18082, https://doi.org/10.1021/ACSSUSCHEMENG.0C06345/SUPPL_FILE/SC0C06345_SL_001.PDF.
 - [17] F. Bougie, D. Pokras, X. Fan, Novel non-aqueous MEA solutions for CO2 capture, Int. J. Greenh. Gas Control 86 (2019) 34–42, <https://doi.org/10.1016/j.ijggc.2019.04.013>.
 - [18] F. Barzaghi, C. Giorgi, F. Mani, M. Peruzzini, Reversible carbon dioxide capture by aqueous and non-aqueous amine-based absorbents: a comparative analysis carried out by 13C NMR spectroscopy, Appl. Energy 220 (March) (2018) 208–219, <https://doi.org/10.1016/j.apenergy.2018.03.066>.
 - [19] H. Guo, C. Li, X. Shi, H. Li, S. Shen, Nonaqueous amine-based absorbents for energy efficient CO2 capture, Appl. Energy 239 (2019) 725–734, <https://doi.org/10.1016/j.apenergy.2019.02.019>.
 - [20] K. Fu, C. Liu, L. Wang, X. Huang, D. Fu, Performance and mechanism of CO2 absorption in 2-ethylhexyl-1-amine + glyme non-aqueous solutions, Energy 220 (2021) 119735, <https://doi.org/10.1016/J.ENERGY.2020.119735>.
 - [21] L. Bihong, Y. Kexuan, Z. Xiaobin, Z. Zuoming, J. Guohua, 2-Amino-2-methyl-1-propanol based non-aqueous absorbent for energy-efficient and non-corrosive carbon dioxide capture, Appl. Energy 264 (2020), <https://doi.org/10.1016/j.apenergy.2020.114703>.
 - [22] H. Svensson, J. Edfeldt, V. Zejnullah Velasco, C. Hultberg, H.T. Karlsson, Solubility of carbon dioxide in mixtures of 2-amino-2-methyl-1-propanol and organic solvents, Int. J. Greenh. Gas Control 27 (2014) 247–254, <https://doi.org/10.1016/J.IJGGC.2014.06.004>.
 - [23] Y. Li, J. Cheng, L. Hu, J. Liu, J. Zhou, K. Cen, Phase-changing solution PZ/DMF for efficient CO2 capture and low corrosiveness to carbon steel, Fuel 216 (December 2017) (2018) 418–426, <https://doi.org/10.1016/j.fuel.2017.12.030>.
 - [24] X. Gao, X. Li, S. Cheng, B. Lv, G. Jing, Z. Zhou, A novel solid-liquid ‘phase controllable’ biphasic amine absorbent for CO2 capture, Chem. Eng. J. 430 (2022) 132932, <https://doi.org/10.1016/J.CEJ.2021.132932>.
 - [25] X. Zhou, X. Li, J. Wei, Y. Fan, L. Liao, H. Wang, Novel nonaqueous liquid-liquid biphasic solvent for energy-efficient carbon dioxide capture with low corrosivity, Environ. Sci. Technol. 54 (24) (2020) 16138–16146, <https://doi.org/10.1021/acs.est.0c05774>.
 - [26] X. Li, X. Zhou, J. Wei, Y. Fan, L. Liao, H. Wang, Reducing the energy penalty and corrosion of carbon dioxide capture using a novel nonaqueous monoethanolamine-based biphasic solvent, Sep. Purif. Technol. 265 (November 2020) (2021) 118481, <https://doi.org/10.1016/j.seppur.2021.118481>.
 - [27] H.K. Karlsson, H. Makhool, M. Karlsson, H. Svensson, Chemical absorption of carbon dioxide in non-aqueous systems using the amine 2-amino-2-methyl-1-propanol in dimethyl sulfoxide and N-methyl-2-pyrrolidone, Sep. Purif. Technol. 256 (2021) 117789, <https://doi.org/10.1016/J.SEPPUR.2020.117789>.
 - [28] F.A. Chowdhury, K. Goto, H. Yamada, Y. Matsuzaki, A screening study of alcohol solvents for alkanolamine-based CO2 capture, Int. J. Greenh. Gas Control 99 (2020), <https://doi.org/10.1016/j.ijggc.2020.103081>.
 - [29] G. Lu, et al., An energy-efficient cyclic amine system developed for carbon capture from both flue gas and air, Chem. Eng. J. 496 (2024) 154085, <https://doi.org/10.1016/j.cej.2024.154085>.
 - [30] F. Bougie, D. Pokras, X. Fan, Novel non-aqueous MEA solutions for CO2 capture, Int. J. Greenh. Gas Control 86 (2019) 34–42, <https://doi.org/10.1016/j.ijggc.2019.04.013>.
 - [31] F. Bougie, X. Fan, Microwave regeneration of monoethanolamine aqueous solutions used for CO2 capture, Int. J. Greenh. Gas Control 79 (July) (2018) 165–172, <https://doi.org/10.1016/j.ijggc.2018.10.008>.
 - [32] S. Zheng, M. Tao, Q. Liu, L. Ning, Y. He, Y. Shi, Capturing CO2 into the precipitate of a phase-changing solvent after absorption, Environ. Sci. Technol. 48 (15) (2014) 8905–8910, <https://doi.org/10.1021/es501554h>.
 - [33] F. Bougie, X. Fan, Analysis of the regeneration of monoethanolamine aqueous solutions by microwave irradiation, Energy Proc. 142 (2017) 3661–3666, <https://doi.org/10.1016/j.egypro.2017.12.259>.
 - [34] G. Lu, et al., Development of novel AMP-based absorbents for efficient CO2 capture with low energy consumption through modifying the electrostatic potential, Chem. Eng. J. 474 (2023) 145929, <https://doi.org/10.1016/j.cej.2023.145929>.
 - [35] G. Jing, Y. Qian, X. Zhou, B. Lv, Z. Zhou, Designing and screening of multi-amino-functionalized ionic liquid solution for CO2 capture by quantum chemical simulation, ACS Sustain. Chem. Eng. 6 (1) (2018) 1182–1191, <https://doi.org/10.1021/acssuschemeng.7b03467>.
 - [36] M.J. Frisch, et al., G16_C01, Gaussian 16, Revision C.01, Gaussian Inc, Wallin, 2016.
 - [37] M.J. Al-Marri, M.M. Khader, E.P. Giannelis, M.F. Shibli, Optimization of selection of chain amine scrubbers for CO2 capture, J. Mol. Model. 20 (12) (2014) 2518, <https://doi.org/10.1007/s00894-014-2518-8>.
 - [38] X. Li, et al., Low energy-consuming CO2 capture by phase change absorbents of amine/alcohol/H2O, Sep. Purif. Technol. 275 (2021) 119181, <https://doi.org/10.1016/j.seppur.2021.119181>.
 - [39] M. Chen, M. Li, F. Zhang, X. Hu, Y. Wu, Fast and efficient CO2 absorption in non-aqueous tertiary amines promoted by ethylene glycol, Energy Fuel 36 (9) (2022) 4830–4836, <https://doi.org/10.1021/acs.energyfuels.2c00215>.
 - [40] C. Yang, M. Liu, J. Zhang, X. Wang, Y. Jiang, J. Sun, Facile synthesis of DBU-based ionic liquids cooperated with ZnI2 as catalysts for efficient cycloaddition of CO2 to epoxides under mild and solvent-free conditions, Mol. Catal. 450 (January) (2018) 39–45, <https://doi.org/10.1016/j.mcat.2018.02.018>.
 - [41] X. Zhu, et al., DBU-glycerol solution: a CO2 absorbent with high desorption ratio and low regeneration energy, Environ. Sci. Technol. 54 (12) (2020) 7570–7578, <https://doi.org/10.1021/acs.est.0c01332>.
 - [42] F.O. Ochedi, J. Yu, H. Yu, Y. Liu, A. Hussain, Carbon dioxide capture using liquid absorption methods: a review, Environ. Chem. Lett. 19 (1) (2021) 77–109, <https://doi.org/10.1007/s10311-020-01093-8>.
 - [43] S. Zhang, Y. Shen, L. Wang, J. Chen, Y. Lu, Phase change solvents for post-combustion CO2 capture: principle, advances, and challenges, Appl. Energy 239 (November 2018) (2019) 876–897, <https://doi.org/10.1016/j.apenergy.2019.01.242>.
 - [44] X. Gao, X. Li, S. Cheng, B. Lv, G. Jing, Z. Zhou, A novel solid-liquid ‘phase controllable’ biphasic amine absorbent for CO2 capture, Chem. Eng. J. 430 (2022) 132932, <https://doi.org/10.1016/j.cej.2021.132932>.
 - [45] C. Liu, et al., Inhibiting effect of 2-amino-2-methyl-1-propanol on gelatinous product formation in non-aqueous CO2 absorbents: experimental study and molecular understanding, Chem. Eng. J. 481 (2024) 148545, <https://doi.org/10.1016/j.cej.2024.148545>.
 - [46] H. Sun, et al., COMPASS II: extended coverage for polymer and drug-like molecule databases, J. Mol. Model. 22 (2) (2016) 47, <https://doi.org/10.1007/s00894-016-2909-0>.
 - [47] H. Sun, P. Ren, J.R. Fried, The COMPASS and validation, Comput. Theor. Polym. Sci. 8 (1) (1998) 229–246.
 - [48] H. Sun, Compass: an ab initio force-field optimized for condensed-phase applications – overview with details on alkane and benzene compounds, J. Phys. Chem. B 102 (38) (1998) 7338–7364, <https://doi.org/10.1021/jp980939v>.
 - [49] B. Aghel, S. Janati, S. Wongwises, M.S. Shadloo, Review on CO2 capture by blended amine solutions, Int. J. Greenh. Gas Control 119 (2022) 103715, <https://doi.org/10.1016/j.ijggc.2022.103715>.
 - [50] G. Puxty, R. Rowland, Modeling CO2 mass transfer in amine mixtures: PZ-AMP and PZ-MDEA, Environ. Sci. Technol. 45 (6) (2011) 2398–2405, <https://doi.org/10.1021/es1022784>.
 - [51] J. Ying, S. Raets, D. Eimer, The activator mechanism of piperazine in aqueous methyldiethanolamine solutions, Energy Proc. 114 (2017) 2078–2087, <https://doi.org/10.1016/j.egyproc.2017.03.1342>.
 - [52] O. Hamdaoui, E. Naffrechoux, J. Suptil, C. Fachinger, Ultrasonic desorption of p-chlorophenol from granular activated carbon, Chem. Eng. J. 106 (2) (2005) 153–161, <https://doi.org/10.1016/j.cej.2004.10.010>.
 - [53] O. Lacin, B. Bayrak, O. Korkut, E. Sayan, Modeling of adsorption and ultrasonic desorption of cadmium(II) and zinc(II) on local bentonite, J. Colloid Interface Sci. 292 (2) (2005) 330–335, <https://doi.org/10.1016/j.jcis.2005.05.092>.
 - [54] J.F. Corbett, Pseudo first-order kinetics, J. Chem. Educ. 49 (10) (1972) 663, <https://doi.org/10.1021/ed049p663>.

- [55] M. Peleg, M.D. Normand, M.G. Corradini, The Arrhenius equation revisited, Crit. Rev. Food Sci. Nutr. 52 (9) (2012) 830–851, <https://doi.org/10.1080/10408398.2012.667460>.
- [56] L. Yin, X. Li, L. Zhang, J. Li, Characteristics of carbon dioxide desorption from MEA-based organic solvent absorbents, Int. J. Greenh. Gas Control 104 (2021) 103224, <https://doi.org/10.1016/j.ijggc.2020.103224>.
- [57] CRC Handbook of Chemistry and Physics, 88th ed Editor-in-Chief: David R. Lide (National Institute of Standards and Technology) CRC Press/Taylor & Francis Group, Boca Raton, FL. 2007. 2640 pp. \$139.95. ISBN 0-8493-0488-1, J. Am. Chem. Soc. 130(1) (2008) 382, doi: 10.1021/ja077011d.
- [58] F. Bougie, D. Pokras, X. Fan, Novel non-aqueous MEA solutions for CO₂ capture, Int. J. Greenh. Gas Control 86 (January) (2019) 34–42, <https://doi.org/10.1016/j.ijggc.2019.04.013>.
- [59] A. García-Abuín, D. Gómez-Díaz, J.M. Navaza, A. Rumbo, Carbon dioxide capture with tertiary amines. Absorption rate and reaction mechanism, J. Taiwan Inst. Chem. Eng. 80 (2017) 356–362, <https://doi.org/10.1016/j.jtice.2017.07.022>.
- [60] M. Chen, et al., A study on reaction mechanism and kinetics of CO₂ and MEA/DEA-tertiary amines in non-aqueous and water-lean solutions, Chem. Eng. Sci. 269 (2023) 118431, <https://doi.org/10.1016/j.ces.2022.118431>.
- [61] M. Chen, H. Gao, T. Sema, M. Xiao, Q. Sun, Z. Liang, Study on the mechanism and kinetics of amine with steric hindrance absorbing CO₂ in non-aqueous/aqueous solution, Sep. Purif. Technol. 303 (2022) 122202, <https://doi.org/10.1016/j.seppur.2022.122202>.
- [62] X.E. Hu, et al., NMR techniques and prediction models for the analysis of species formed in CO₂ capture processes with amine-based sorbents: a critical review, ACS Sustain. Chem. Eng. 8 (16) (2020) 6173–6193, <https://doi.org/10.1021/acssuschemeng.9b07823>.
- [63] J. Davis, G. Rochelle, Thermal degradation of monoethanolamine at stripper conditions, Energy Proc. 1 (1) (2009) 327–333, <https://doi.org/10.1016/j.egypro.2009.01.045>.
- [64] I.O. Furtado, et al., Combined theoretical and experimental studies on CO₂ capture by amine-activated glycerol, Chem. Eng. J. 408 (2021) 128002, <https://doi.org/10.1016/j.cej.2020.128002>.
- [65] C. Zhang, et al., Single atom solutions for carbon dioxide capture, J. Chem. Phys. 158 (8) (2023) 84309, <https://doi.org/10.1063/5.0132627>.
- [66] Y. Wu, C. Zhou, Y. Li, Y. Yu, Z. Zhang, G. Wang, Direct Air Capture carbon dioxide by the 2D single atom solution compressor, Sep. Purif. Technol. (2024) 128442, <https://doi.org/10.1016/j.seppur.2024.128442>.
- [67] C. Ling, Q. Li, A. Du, J. Wang, Computation-aided design of single-atom catalysts for one-pot CO₂ capture, activation, and conversion, ACS Appl. Mater. Interfaces 10 (43) (2018) 36866–36872, <https://doi.org/10.1021/acsami.8b10394>.
- [68] C. Zhou, et al., Single-atom solutions promote carbon dioxide capture, Appl. Energy 332 (2023) 120570, <https://doi.org/10.1016/j.apenergy.2022.120570>.